Tectonophysics 588 (2013) 154–170

Contents lists available at SciVerse ScienceDirect

Tectonophysics

journal homepage: www.elsevier.com/locate/tecto

# Fracture networks and strike–slip deformation along reactivated normal faults in Quaternary travertine deposits, Denizli Basin, western Turkey

Koen Van Noten [a,*], Hannes Claes [a], Jeroen Soete [a], Anneleen Foubert [a], Mehmet Özkul [b], Rudy Swennen [a,**]

[a] Geodynamics and Geofluids Research Group, Department of Earth and Environmental Sciences, Katholieke Universiteit Leuven, Celestijnenlaan 200E, B-3001 Leuven, Belgium
[b] Department of Geological Engineering, Pamukkale University, 20070 Kınıklı Campus, Denizli, Turkey

ARTICLE INFO

*Article history:*
Received 6 June 2012
Received in revised form 3 December 2012
Accepted 10 December 2012
Available online 28 December 2012

*Keywords:*
West Anatolian Extensional Province
Extensional fracturing
Colour-banded calcite veins
Strike–slip faulting
Paleostress analysis

ABSTRACT

The Denizli Basin in the West Anatolian Extensional Province in western Turkey is known for its numerous Quaternary travertine occurrences. Travertine morphology is often dependant on the relative position of the deposition with respect to basin-bounding faults. The travertine occurrences examined in this study are situated at the intersection of the locally E–W oriented Denizli Basin and the adjacent NE–SW oriented Baklan Graben in the NE. Based on an extensive field campaign, including LIDAR scanning, several high-resolution fault/fracture maps of five large quarries (>300 m in length and >60 m in height) are constructed in which this world-class travertine deposit is currently excavated. A structural analysis is performed in order to determine the tectonic overprinting of the travertine body and to derive the stress states of the basin after travertine deposition. The mostly open, non-stratabound joints are several tens of metres long and often bifurcate creating a dense fracture network. Minor infill of the joints resulted in the presence of a few colour-banded calcite veins. Based on the E–W, NE–SW and NW–SE orientation of three dominant joint sets it is concluded that the joint network is caused by local N-S extension, alternated by NW–SE and NE–SW extension exemplifying the presence of stress permutations in the Quaternary. High angle E–W to WNW–ESE faults cross-cut the quarries. Faults are filled with travertine debris and clastic infill of above lying sedimentary units indicative of the open nature of the faults. The specific E–W fault orientation in the locally E–W trending Denizli Basin indicates that they initiated as normal faults. A paleostress inversion analysis performed on kinematic indicators such as striations on the clayey fault infill and the sinistral displacement of paleosols shows that some of the normal faults were reactivated causing left-lateral deformation in a transient strike–slip stress field with a NE–SW oriented $\sigma_1$.



## 1. Introduction

Travertines have been studied in many places around the world, along which well-known examples in Yellowstone National Park (USA), Utah (USA), Central Apennines (Italy), New Zealand and western Turkey. In the last two decades numerous studies on recent Quaternary travertine deposits demonstrated the close relationship between neotectonic activity, hydrothermal circulation and travertine deposition (e.g. Altunel and Hancock, 1993a,b; Brogi and Capezzuoli, 2009; Brogi et al., 2010, 2012; Çakır, 1999; Hancock et al., 1999; Özkul et al., 2002, 2010). These studies particularly focus on understanding the hydrological, microbiological, palaeoclimatological, sedimentological and tectonic aspects that are related to travertine formation. Travertine deposits often have a complex internal sediment architecture frequently changing both in lateral and vertical directions over a short distance. Their complexity originates from many factors such as spring position, underlying topography, hill slope, chemical composition of travertine depositing waters, microbial activity and surficial waters (Guo and Riding, 1998; Özkul et al., 2002). In tectonic active regions, travertines have been described to develop in the hangingwall of normal faults (e.g. Brogi, 2004; Brogi and Capezzuoli, 2009; De Filippis and Billi, 2012), at the ends of fault segments (e.g. Çakır, 1999), in tensional fractures in shear zones (e.g. Faccenna, 1994; Faccenna et al., 2008) and in extensional step-over zones between the offset of normal faults (e.g Altunel and Hancock, 1993a; Brogi et al., 2012; Çakır, 1999; Hancock et al., 1999). With respect to these tectonic settings, the proposed term "travitonics" (Hancock et al., 1999) has become a very useful term to describe this active link between tectonic deformation and travertine development. Importantly, analysing the relationship between travertine build-up and intersecting faults and fractures is very useful for estimating the historical seismicity during basin development. Moreover, the results of paleostress analyses of structural features cutting through travertine deposits (e.g. Çakır, 1999; Kaymakçı, 2006) may be correlated to active tectonic regimes

* Correspondence to: K. Van Noten, Seismology Section, Royal Observatory of Belgium, Ringlaan 3, B-1180 Brussels, Belgium. Tel.: +32 2 790 39 18.
** Corresponding author.
*E-mail addresses:* koen.vannoten@oma.be (K. Van Noten), rudy.swennen@ees.kuleuven.be (R. Swennen).

0040-1951/$ – see front matter © 2013 Elsevier B.V. All rights reserved.
http://dx.doi.org/10.1016/j.tecto.2012.12.018

that are recorded by earthquake seismicity and GPS monitoring (e.g. Aktar et al., 2007).

A travertine fissure ridge is the most common example of a travertine deposit in which Ca-bicarbonate hydrothermal fluids are provided by a single hydrothermal feeder system. The ridge morphology has been described from well-known examples in western Turkey and in Central Italy (Altunel and Hancock, 1996; Altunel and Karabacak, 2005; Brogi and Capezzuoli, 2009; Çakır, 1999; De Filippis et al., 2012; Mesci et al., 2008). Although the formation of travertine has been studied in many tectonic settings, travertine is less investigated when it occurs at the complex intersection of several graben structures. At such intersections, however, a high groundwater permeability, which has been demonstrated by several hydrogeological investigations (e.g. Özer, 2000), is often present and allows the build-up of complex travertine bodies. At the intersection of several fault systems, the deposition of travertine is thus often a consequence of a complex fault- and fracture network in the subsurface, providing the necessary pathways for hydrothermal fluids to ascend.

In this study the geometry of a fault/fracture network developed in a large-scale, extremely well exposed 2 km-wide travertine body is documented. This travertine body is quarried in the southeastern part of the extensional Denizli Basin (western Anatolia, Turkey), at the intersection of three graben structures. Although the quarries exploit a large area of travertine ($>10$ km$^2$) this region has received little attention and has only been studied for its mammal fauna (Erten et al., 2005) and Homo Erectus founds (Kappelman et al., 2008). A brief sedimentological description of the travertine build-up is presented in Özkul et al. (2002) and technical geomechanical properties of construction stones are provided by Çobanoğlu and Çelik (2012) and Yagiz (2010). The quarry area, however, offers a unique possibility to study the complex sedimentological development of travertine and regional neotectonic Quaternary brittle deformation. Based on extensive fieldwork including LIDAR scanning, several high resolution fault/fracture quarry maps are presented. It is particularly focused on brittle structures such as joints, fractures and faults in order to reconstruct the Quaternary deformation history of the study area.

This structural analysis on post-travertine faults and fractures is performed to infer the different local paleostress directions that have been active after travertine deposition in order to understand the neotectonic activity in this area. This topic is of specific importance in the field of tectonics acting in geothermal environments in which travertine formed from tectonically controlled fluid flow. To be able to work out a good sedimentary model, which is beyond the scope of this study, first the effect of the tectonic overprinting needs to be addressed. This study can then be used to determine whether the complex sedimentological build-up of the travertine, which will be elaborated in parallel sedimentological and geochemical studies, fits in one of the deduced paleostress directions.

## 2. Geological and tectonic setting

The active continental extensional deformation of western Anatolia (West Turkey), one of the most seismically active tectonic regions on Earth, has been well described and numerously debated. The extensional basins in the West Anatolian Extensional Province in western Turkey result from a complex intraplate tectonism caused by both the northern migration of the Arabian microplate into the eastern Anatolian plate and the rollback subduction of the North African oceanic crust below the Anatolian plate in the Aegean region (Doutsos and Kokkalas, 2001; Westaway, 1993). On the one hand, the northward migration of Arabia forced the Anatolian block to wedge sideways between the Eurasian and African continent (Bozkurt, 2001; van Hinsbergen et al., 2010; Westaway et al., 2005). The resulting lateral motion causes lateral transpressional and transtensional deformation in the Anatolian Block such as exemplified by several intraplate strike–slip faults and the dominantly dextral and sinistral interplate strike–slip motions along the North Anatolian and East Anatolian fault zones respectively (Fig. 1a). The rollback subduction in the west, on the other hand, has caused an important N–S extension in the West Anatolian Extensional Province that is accompanied by normal faulting and the development of many E–W oriented basins in western Turkey (Demircioğlu et al., 2010; Koçyiğit, 2005; Koçyiğit and Deveci, 2007). Both previously mentioned geodynamic processes triggered the orogenic collapse of the Menderes Massif in the Miocene and caused the Pliocene to Quaternary development of the main E–W grabens and NW–SE or NE–SW cross-grabens in western Turkey (Westaway, 1993; Westaway et al., 2005). Different combinations of previous described geodynamic models have, however, been proposed and are summarised in Van Hinsbergen et al. (2010) and Gürbüz et al. (2012). As demonstrated by (current) seismic activity within the West Anatolian Extensional Province, many destructive earthquakes with a dominant normal fault activity have occurred within these E–W grabens (Aktar et al., 2007; Taymaz and Price, 1992). Only minor strike–slip faulting has been monitored at the intersection of some large-scale grabens (Aktar et al., 2007; Bozkurt and Sözbilir, 2006).

The currently still active Denizli Basin, located in the eastern part of the West Anatolian Extensional Province (Fig. 1b), developed in Cycladic blueschists, Cretaceous HP-LT nappes and Oligocene and Neogene sediments (van Hinsbergen et al., 2010). In the northern part of the basin, basement rocks dominantly consists of crystalline limestones (Westaway, 1993). A detailed stratigraphy of these pre-Neogene and Neogene deposits is described in Alçiçek et al. (2007). The Bouguer anomalie reflects the structure of a graben in which higher densities demonstrate the presence of metamorphic rocks below the Neogene deposits in the Denizli Basin (see Özgüler et al., 1984). The NE–SW oriented Denizli Basin is *c.* 50 km long and *c.* 24 km wide and is bounded by major NNE-dipping normal faults at its southwestern border and SSW-dipping normal faults at its northeastern border. According to Westaway (1993), extension in the Denizli Basin began in the Middle Miocene and has been active ever since.

The western part of the Denizli Basin is situated in a tectonic area at the intersection of three major E–W grabens. Laterally, it forms the continuation of the Büyük Menderes Graben and is separated by a topographic high from the Küçük Menderes and Gediz Grabens (Kaymakçı, 2006) (Fig. 1b). The central part of the Denizli Basin is characterised by a typical horst-graben structure and comprises two Quaternary sub-basins, namely the Laodikeia Graben in the south and the Çürüksu Graben in the north (Kaymakçı, 2006; Koçyiğit, 2005). This horst-graben morphology has been formed due to subsidence in the Denizli Basin, accompanied by several phases of tectonic uplift along the horsts (Westaway et al., 2005). The northern border of the Çürüksu Graben is the well-defined NW–SE Pamukkale Fault Zone that extends several tens of kilometres (Fig. 1c). Along this fault zone, travertine occurrences, among which the famous Pamukkale travertine (a UNESCO World Heritage Site), are precipitated in kilometre-wide left-lateral step-over zones that are developed between different NW–SE normal faults (Altunel and Hancock, 1993a; Çakır, 1999). The overall NW–SE orientation of the Denizli Basin curves towards an E–W orientation in its southwestern part, forming the lateral extend of the eastern NE–SW Baklan Graben and the E–W to NE–SW Acıgöl Graben (Fig. 1c) (Koçyiğit and Deveci, 2007). The eastern end of the Denizli Basin has a staircase geometry at the major Honaz and Kaklık faults, along which the Baklan, Acıgöl and Acıpayam basin-bounding faults interfere (Kaymakçı, 2006). In this region smaller antithetic faults trending N–S are intersected by the Honaz and Kaklık faults. Both the adjacent Baklan and Acıgöl Grabens are characterised by a halfgraben morphology due to greater subsidence rates at the southern basin-bounding faults (Price and Scott, 1994).

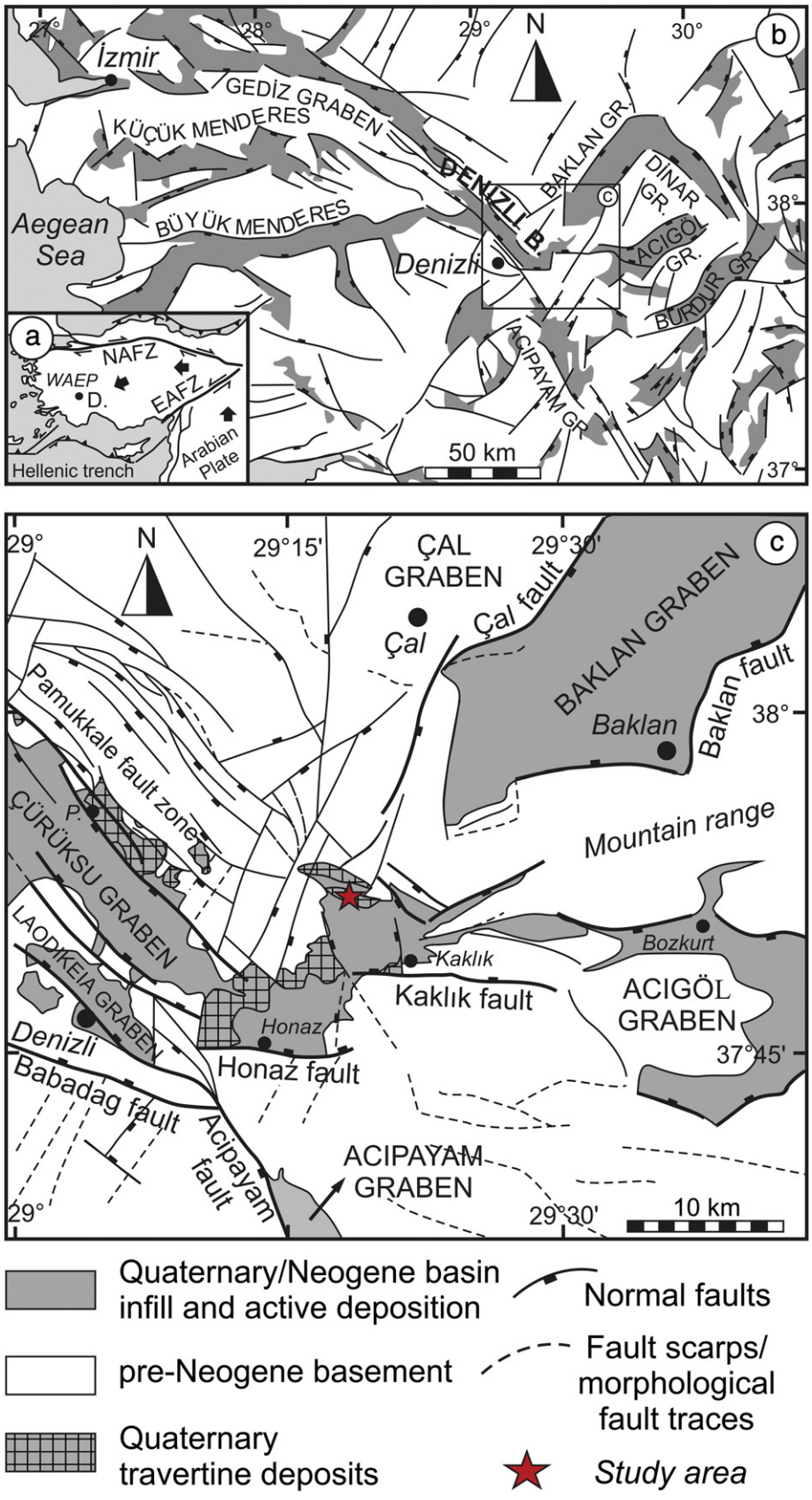


**Fig. 1.** Geodynamic setting. Map orientations are in UTM coordinates (UTM Zone 35, WGS 84). (a) Simplified tectonic map of Turkey. Owing to the northwards migration of the Arabian plate and the northwards subduction of the Hellenic trench, the Anatolian block is extruded westwards resulting in right- and left-lateral deformation respectively along the North Anatolian (NAFZ) and East Anatolian Fault Zone (EAFZ). WAEP: West Anatolian Extensional Province; D.: Denizli Basin. (b) The N–S extension in the WAEP drives the formation of several larger E–W oriented basins and relatively small NW–SE to NE–SW trending cross-basins. After Kaymakçı (2006). (c) The Denizli Basin has a horst-graben morphology that is composed of two Quaternary sub-basins, namely the Çürüksu and Laodikeia grabens. Major basin-bounding NW–SE, E–W and NNE–SSW oriented fault zones form the current shape of the Denizli Basin. The study area is situated at the intersection of the local E–W trending Denizli Basin and adjacent Baklan and Acıgöl Grabens. Map constructed from Landsat ETM images and SRTM data after Kaymakçı (2006), Gürbüz et al (2012), Koçyiğit and Deveci (2007). P.: Pamukkale.

The studied travertine deposits are located in the southeastern part of the Denizli Basin, more specifically in the northern part of the local E–W trending Denizli Basin. They are exposed in several aligned quarries in the Ballık area situated approximately 6 km NW of a little village Kaklık (Fig. 1c). The study area is characterised by the north-dipping Kaklık fault in the south, the prolongation of the NW–SE Pamukkale Fault Zone in the west, and the Çal and Baklan faults, i.e. the basin-bounding faults of the Baklan Graben, in the NE (Fig. 1c). The presence of dominantly normal faults has played an important role in slope development and the typical morphology of these (half)grabens. However, due to the intersection of several graben-bounding faults, the graben morphology around the studied travertine body is even more complex, possibly due to the differential Quaternary uplift of different fault blocks (Westaway et al., 2005).

Topographically, the study area can be separated in a northern upper area, in which several quarries ($n>10$) excavate the south-dipping northern graben edge of the locally E–W trending Denizli Basin, and a lower 'domal area', forming a *c.* 70 m topographical high above the local flat basin floor. The travertine in this region has gained a stepped structure from north to south (Fig. 2) which is related to normal faulting along the graben edge (Özkul et al., 2002). Worth mentioning are the Quaternary Tosunlar Formation and the middle Late Miocene Kolankaya Formation on which the travertine is developed (Alçiçek et al., 2007). The basin floor of the locally E–W oriented Denizli Basin is constituted of the Tosunlar Formation. It consists of alternating continental deposits such as conglomerate, sandstone, mudstone and marls that sometimes laterally emerge into the travertine. The Kolankaya Formation consists of claystone, siltstone, marl, limestone, black shale, conglomerate and sandstone, a lithology representative of a changing depositional environment from deep lake to foreshore and alluvial deposits (Alçiçek et al., 2007).

The domal area is currently excavated by six large travertine quarries that form the subject of this study. In a clockwise orientation these quarries have the following names: the Abandoned, Alimoğlu, Çakmak, İlik, Faber and Ece quarries (Fig. 2). In each quarry the flow direction of the travertine is towards the external part of the domal area, giving rise to a domal structure. An explanation for the important and particular lenticular shape of this domal area has thus to be found in the complex sedimentological build-up of the travertine body. A detailed sedimentological reconstruction of the travertine deposition, however, lies beyond the structural goal of this study.

## 3. Methodology

The different quarries were investigated during an extensive field survey in the summer of 2011. It was particularly focused on the geometric analysis of brittle structures such as joints, veins and faults. In this paper the term *joint* is specifically used for all extension fractures along which no displacement has been observed. The term *fracture* refers to any discontinuity in the rock mass along which displacement occurs, or when it is unclear if there is displacement. Orientation of joints, fractures, faults and kinematic indicators were measured with a Freiberger structural geological compass. The orientation of planar features (joints, faults) is reported as dip direction/dip (*e.g.* 180/80 for a plane dipping steeply to the south) and the orientation of linear features (slickenlines, stress axes) is reported as trend/plunge (*e.g.* 270/20 for a slickenline plunging to the west). The joint and fault orientations, which are illustrated for each quarry, are plotted in a lower-hemisphere, equal-area stereographic projection by using the analysis program Stereo 32 (Röller and Trepmann, 2003). Particular kinematic indicators on fault surfaces, such as slickenlines on slip surfaces, were used to determine the kinematics of the different faults. Larger bedding structures such as horizontal laminar travertine or paleosols were useful for correlating small-scale kinematic observations with large-scale fault displacements.

Due to continuously changing excavation fronts and absence of detailed quarry maps, individual fault observations were recorded by using a Trimble Geoexplorer GPS. This apparatus allowed recording high-accuracy GPS points. Subsequently, detailed high resolution fault/joint maps were made by plotting the GPS points on orthogonal map projections based on the LIDAR scanning data. The described faults and fractures are numbered according to their first observed occurrence on the different excavation levels: e.g. L1.100 is the first fault or fracture observed on level 1; L2.100 is the same fault but observed on level 2. In this numbering '100' refers to the first fault or joint observed on level 1. L1.112 would then refer to the 12th fault or joint observed on level 1. This field numbering was used to easily recognise similar faults or fractures on different levels.

In a next step, a paleostress analysis was performed on the collected fault-slip data. The method used allows a fault-slip data inversion which involves the concept of the best-fitting stress tensor, capable of explaining the direction of slip on the studied faults. The paleostress tensor and the principal stress directions responsible for the (re)activation of the observed faults were derived from the Right Dihedral Method (Angelier and Mechler, 1977) optimised in the Win-Tensor Program (version 4.0.4), a software developed by Dr. D. Delvaux (Royal Museum for Central Africa, Belgium) (Delvaux and Sperner, 2003). This program has the advantage that different phases of faulting can be separated manually and automatically, giving rise to a semi-automatic solution.

## 4. Travertine morphologies

The deposits in the quarries NW of Kaklık are discontinuous both in lateral and vertical direction and display white travertine, greenish gray, cream-coloured lake-marsh deposits, reddish-brown coloured alluvium, paleosols and coarse-grained ephemeral river sediments

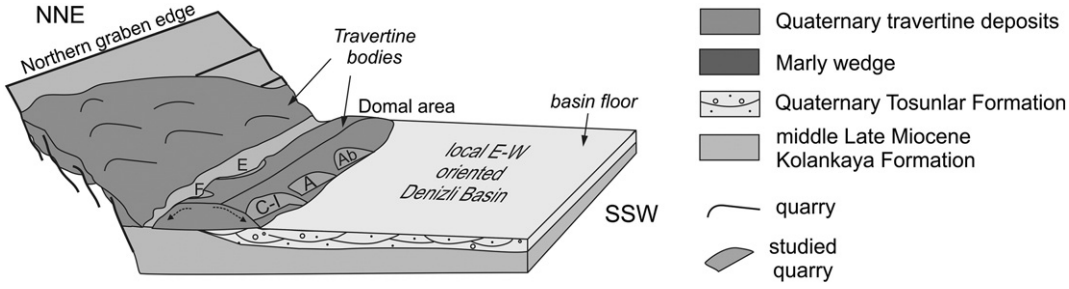


**Fig. 2.** Conceptual sketch of the study area illustrating the position of travertine bodies at the northern graben edge of the locally E–W oriented Denizli Basin. Quaternary travertine deposits are developed on top of Quaternary and middle Late Miocene sedimentary deposits. The quarries in the travertine body on the northern graben edge, which is characterised by normal faults, have not been studied. This study focuses on the domal area which particular shape is related to the flow direction (arrows) of the travertine. Studied quarries in the domal area are the Çakmak and İlik quarries (C-I), the Alimoğlu quarry (A), the Abandoned quarry (Ab) and the Faber (F) and Ece (E) quarries. Figure not to scale.

(Özkul et al., 2002). The age of the oldest travertine deposits has not been clarified yet. The age of first travertine accumulation at Pamukkale are at least 400,000 years old and late Pleistocene in age (Altunel and Hancock, 1993a,b, 1996). Although it is not intended to describe the sedimentological architecture of the geobody in detail, the different recognised travertine deposits are shortly described in order to inform on the specific rock structure in which joints, fractures and faults are developed. A more detailed lithofacies description can be found in the facies classification of Guo and Riding (1998). Horizontally bedded travertine, representative of horizontal deposition, is present at the lower quarry levels in all quarries. This rock structure is dominated by small-scale pores of which many are non-connected (Fig. 3a). Sometimes secondary calcite minerals partially fill up these pores. Towards the middle part of the quarries the horizontally bedded travertine is overlain by white to yellow-brown reed mould travertine (Fig. 3b). Undulating cascade travertine (Fig. 3c) and steep waterfall travertine (Fig. 3d) are examples of slope travertine deposits. The cascade travertine is indicative of a gentle slope environment in which water flows in a laminar condition. It laterally can evolve into small pools and rims such as observed at the active travertine deposits at Pamukkale. Waterfall travertine is often accompanied by plant imprints (such as hanging bryophytes and macrophytes) which were present during precipitation. Sometimes a debris infill facies is present in between opposite oriented cascades and waterfalls. The travertine and siliciclastic layers at the edges of the quarries are characterised by gently dipping, layered travertine corresponding to a typical "margin facies" in which marly and clayey wedges laterally emerge. In the upper levels of the Çakmak, Faber and Ece quarries several metre-wide primary cavities occur in which "stalactite-like" structures have formed due to calcite coating around pending bryophyte structures (Fig. 3e; e.g. Özkul et al., 2010). At the bottom of these cavities accumulations of calcite rafts frequently occur, indicative of precipitation in stagnant waters (Jones and Renaut, 2010). At the top of the Çakmak and İlik quarries, the travertine geobody is overlain by a clastic sequence, i.e. a polymict conglomerate. The conglomeratic level is often unconsolidated, which defines it as gravel, and has a variety in pebble composition such as marl, limestone, chert and serpentinite.

Detailed mapping of the travertine geobody architecture revealed that travertine deposition was not continuous through time. This discontinuity is for instance reflected in the İlik quarry by the gently SW-dipping cascade travertine that is overlain by horizontally layered travertine. Such unconformities separating different travertine deposits have been reported to be influenced by the deactivation of thermal springs and/or the change of the water flux (e.g. De Filippis et al., 2012). Alternatively, different travertine precipitation episodes might alternate with tectonic activities in the basin during which the main travertine body is tilted towards the main Denizli Basin as result of fault activity. This would also create an unconformity in the travertine body. The presence of a 0.5 m thick clayey paleosol at level 3 of the Alimoğlu quarry and colluvial deposits between cascade and waterfall lithofacies further emphasise the discontinuity in travertine precipitation. Marly wedges in the western corner of the Çakmak quarry (level 5) show that the travertine body is laterally limited.

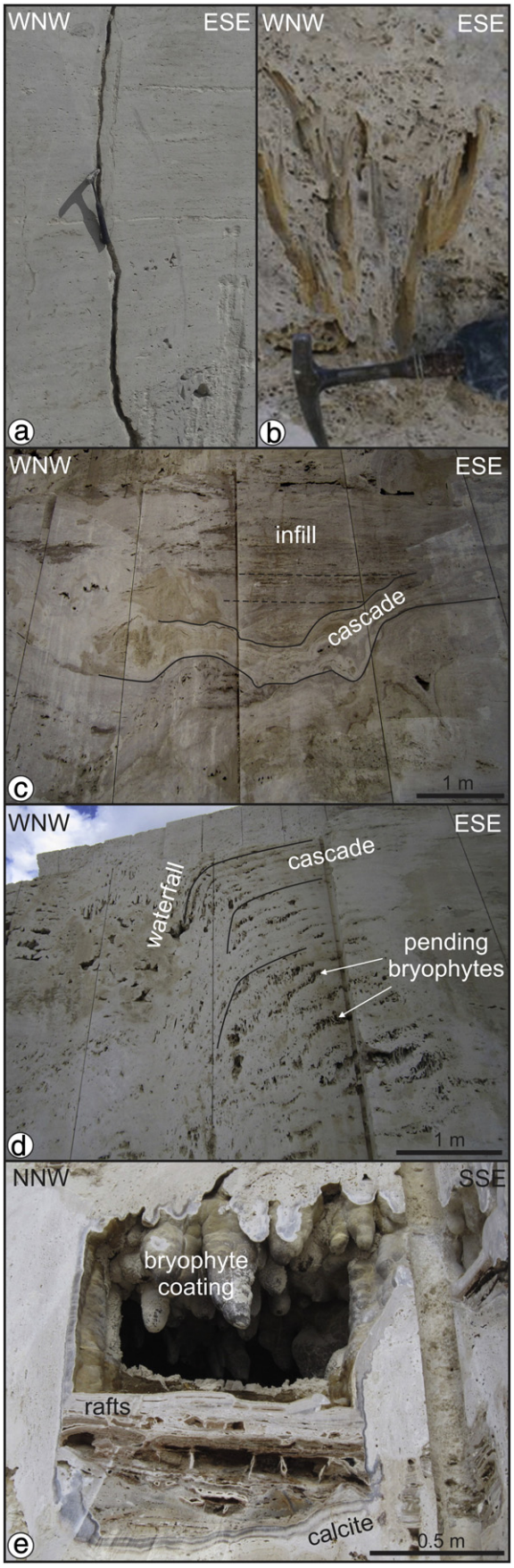


**Fig. 3.** Travertine lithofacies. See Figs. 4, 9 and 12 for picture localisation. (a) Horizontally layered travertine from the lower levels in the quarries. Hammer (32 cm) for scale. Level 1, Çakmak quarry. (b) Reed mound lithofacies. Hammer (32 cm) for scale. Level 4, Çakmak quarry. (c) Undulating cascade lithofacies covered with travertine debris. Level 5a, Çakmak quarry. (d) Cascade lithofacies evolving to waterfall lithofacies. Travertine precipitated around pending bryophyte structures. Level 5a, Çakmak quarry. (e) Metre-wide cavity characterised by stalactite-like structures at the top and calcite rafts at the bottom. These structures consist of calcite encrusted bryophyte plants with additional calcite coating. Notice that the secondary calcite precipitation surrounds the entire cavity. Southernmost part of Level 7, Faber quarry.

## 5. Fault/fracture analysis in the domal area

### 5.1. Alimoğlu and Abandoned quarries

The NW–SE oriented Alimoğlu quarry is approximately 500 m long and 150 m wide. The different quarry walls are currently excavated in 9 levels of which the height of each quarry wall varies between 2 m and 10 m. The quarry is excavated in large blocks of approximately 12 $m^3$. Due to several faults cross-cutting the quarry a lot of waste rock has to be removed during the excavation. The N–S oriented Abandoned quarry east from Alimoğlu is the easternmost studied quarry. It is an approximately 200 m long and 100 m wide quarry and forms the eastern prolongation of the Alimoğlu quarry (Fig. 4).

#### 5.1.1. Joint orientation, morphology and infill

The measured joints on levels 1 to 6 can be divided in three distinct, mutual abutting joint sets. The two dominant joint sets have a general E–W and NE–SW orientation. Only a minority of joints belongs to the third NW–SE set (Fig. 4). There is also a spatial difference in joint distribution: the NE–SW set is more abundant in the centre of the quarry, whereas the E–W set occurs more often at the eastern edge of the quarry. Joint height ranges from one to several metres, often spanning the excavation levels (Fig. 5a). If the height exceeds the excavation level, the joint prolongation can only seldom be traced between the different levels suggesting that joint length and height are rather limited to a couple of metres. Joint traces range from single planar fractures to anastomosing, strongly bifurcating fractures with typical millimetre-size opening and irregular fracture walls. Sometimes, joint opening increases up to maximum sizes of several tens of centimetres. Majority of joints are open travertine fissures without any displacement along the fracture walls, independent to which joint set the joint belongs. Infill of white travertine powder is often observed but is probably related to the infiltration of crushed travertine during excavation. A considerable amount of iron oxide is present in the powder infill, giving the joint filling a brown oxidised appearance. With respect to the different recognised travertine lithofacies, the horizontally bedded travertine in the lower levels and the "margin facies" at the edges of the travertine body are more densely fractured (higher joint density) than the reed mound, cascade and waterfall lithofacies. This gives the "margin facies" a typical irregular appearance (Fig. 5b) in which joints change in orientation from steeply dipping to parallel to layering. It is therefore much easier to trace a joint in the laminar lithofacies from one level to another than in other lithofacies in which fracturing is more irregularly distributed.

#### 5.1.2. Fault orientation, morphology and kinematics

Eleven WNW–ESE to NW–SE trending faults have been observed in the Alimoğlu and the Abandoned quarry (Fig. 4). These high-angle, nearly vertical faults are several hundreds of metres long and some of them can be traced between both quarries (e.g. fault lengths of L3.312 and L3.322 > 600 m). A fault may bifurcate along its length (e.g. L3.322) or may comprise two fault cores with in between an internal undamaged travertine part (e.g. L3.300). Fault thickness is often variable along the fault height (e.g. Fig. 6a) ranging between 0.5 m and 2.5 m. The infill is dominated by travertine clasts up to 0.5 m originating from the adjacent fault walls (Fig. 6a, b and c). The internal lamination in the clasts shows that they are slightly rotated in the fault (Fig. 6b). Several faults (L3.300, L3.700) are characterised by the presence of vertical, dark organic sedimentary layers, probably rich in manganese oxides. With respect to the rather white layered travertine, the travertine clasts in the fault walls are often marked by colour alteration due to weathering. In the Alimoğlu

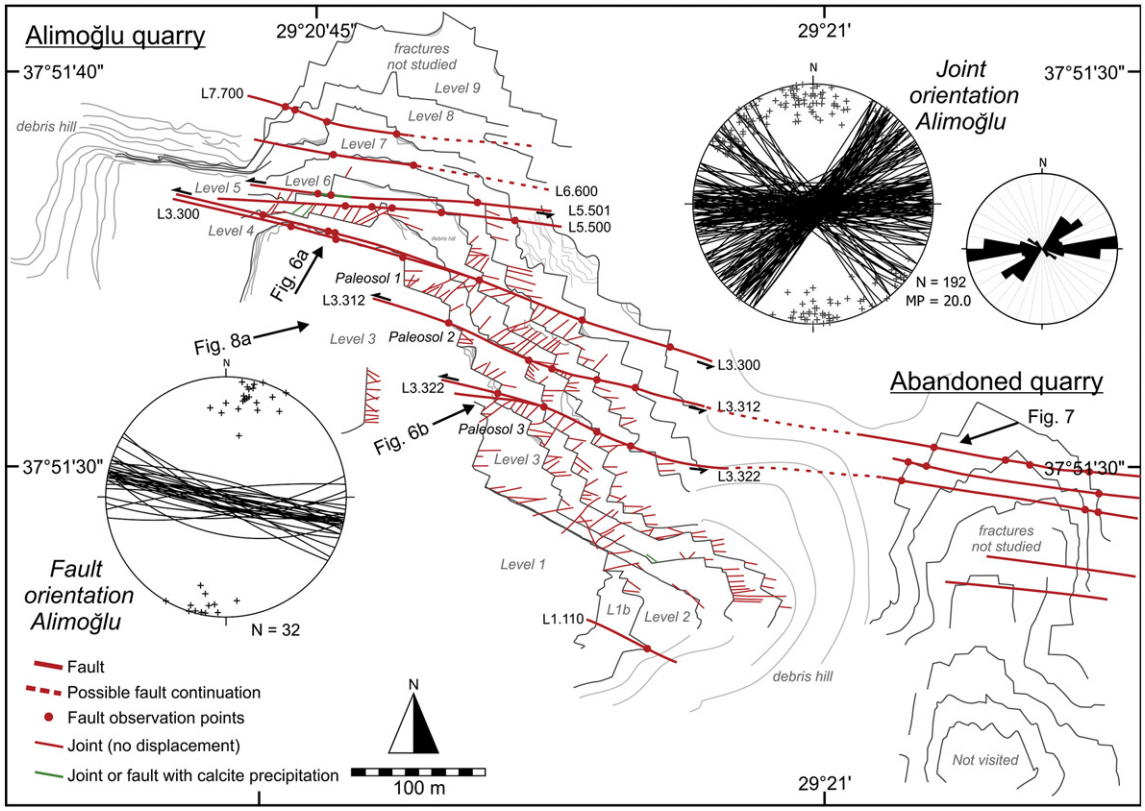


**Fig. 4.** Detailed fault/fracture map of the Alimoğlu and the adjacent Abandoned quarry. Joint and fault orientation are displayed on lower-hemisphere, equal-area stereographic projections. Joints at level 7, 8 and 9 are not studied. Faults L3.300, L3.312, L3.322 and L5.501 are demonstrated to be oblique-slip and strike–slip faults with a sinistral displacement. The rose diagram displays joint orientation and visualises three distinct joint sets. Sector size is 10°. Maximum percentage (MP) marks the perimeter.

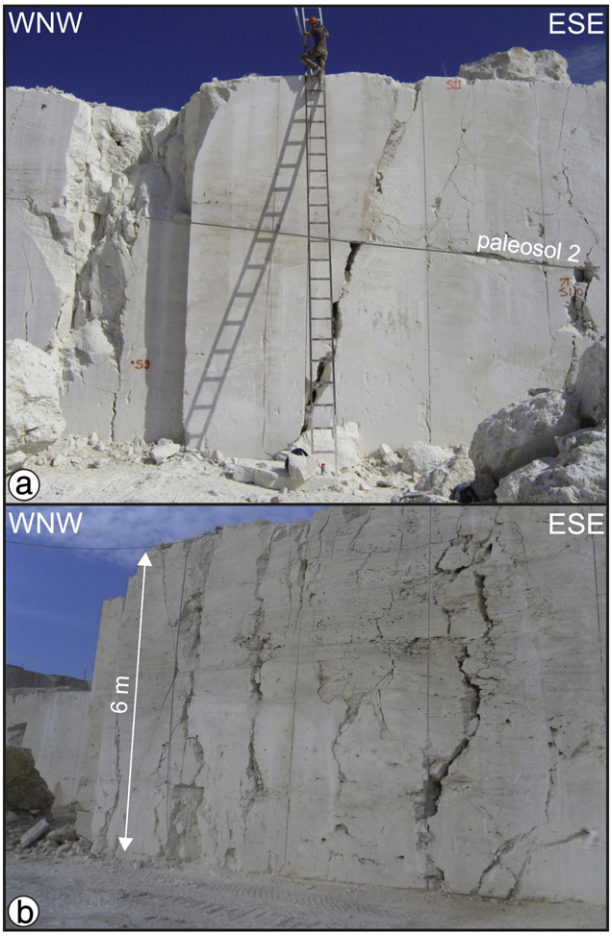


**Fig. 5.** Joint morphology of selected joints in the Alimoğlu quarry. (a) 6 m high joint with a 15 cm opening. Geologist (1.88 m) for scale. (b) Typical irregular joint pattern in the margin facies.

quarry only fault L5.501 bears evidence of restricted fluid flow along the fault. This is exemplified by several white-brown colour-banded calcite infill of unknown origin that precipitated on the fault walls and grows towards the centre of the fault (Fig. 6c, d and e). The absence of calcite veins in the other faults indicates that faulting occurred in rather dry circumstances and in absence of channelised fluid flow. Between the clasts, the faults are filled by brown oxidised clay on which slickenlines can be observed (Fig. 6f). There is no evidence of a damage zone around the faults indicating that deformation is restricted to displacement along the fault plane.

In the Abandoned quarry, fault L3.312 contains several travertine clasts and is filled with oxidised clays (Fig. 7a). Along the northern vertical fault wall a thick (>0.20 m) colour-banded columnar calcite speleothem is present (Fig. 7b and c). Especially the columnar stalactite morphology of this fault infill (Fig. 7b) suggests that infiltrating water, from which the speleothem precipitated, originates from a descending fluid of unknown origin.

Two faults in the Alimoğlu quarry contain clear evidence to perform a kinematic analysis (Fig. 8a, b and c). Fault L3.300 (visible on levels 3, 4 and 5) and L5.501 (visible on levels 4, 5 and 6) are characterised by slickenlines that are marked on internal clayey fault slip planes. The slickenlines and their corresponding stereoplots

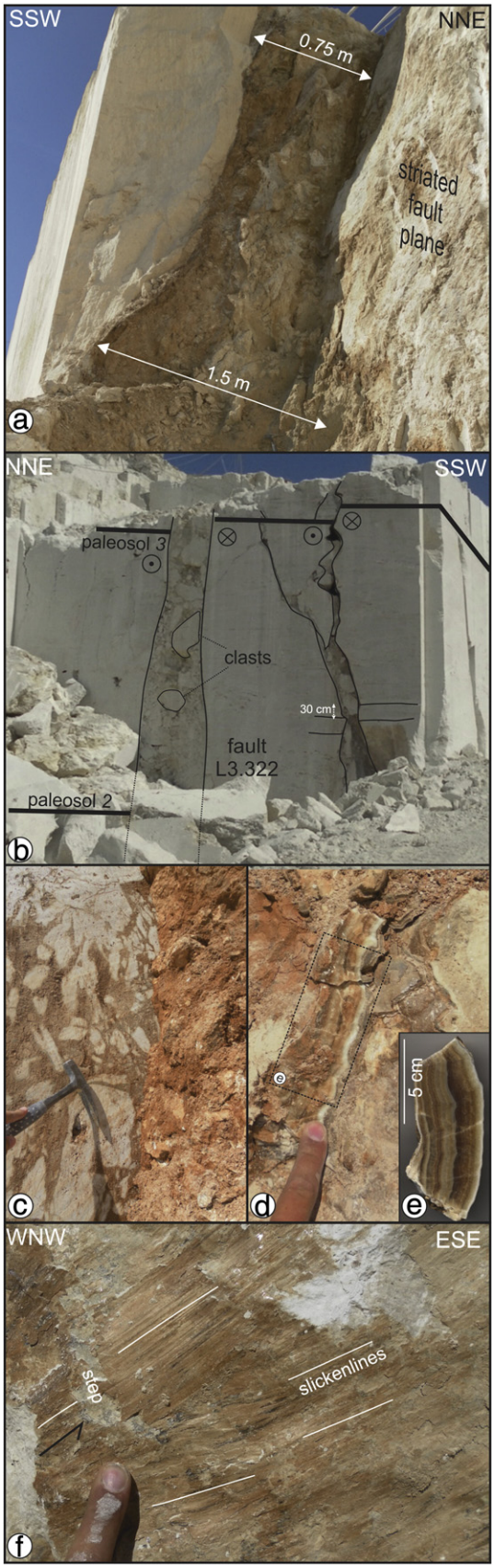


**Fig. 6.** Fault morphology in the Alimoğlu quarry. See Fig. 4 for picture localisation. (a) South-dipping L3.300 fault with variable fault thickness. (b) 1.5 metre-wide fault (L3.322) displacing paleosol 3 at level 3. (c) Infill of fault L5.501, characterised by rotated, decimetre travertine blocks embedded in white to oxidised brown clays. (d) Fault mineralisation in the L5.501 fault. (e) Cut sample of (d) showing the typical white-brown colour-banding of mineralisation internally in the fault. (f) Detail of the striated clayey fault plane in (a) showing gently WNW-plunging slickenlines. The fibre step at the left indicates a left-lateral fault displacement.


**Fig. 7.** (a) Irregular high-angle faults in the Abandoned quarry with (b) speleothems at the northern fault wall. The stalactite morphology of the columnar calcite precipitation demonstrates that the precipitation originates from descending fluids. (c) Detail of (b) showing typical colour-banding that locally can reach a thickness of 20 cm.

are illustrated on Fig. 8b. Along the fault plane of L3.300 five fault segments have been analysed (*1–5* on Fig. 8b). Most internal slip planes are nearly vertical and strike WNW–ESE to NW–SE. These slip planes contain gently to steeply, NW- to W-plunging slickenlines (Fig. 6f). Few slip planes, however, do not correspond to this general trend and are rather strangely W- or S-dipping (Fig. 8b). Some of the slickenlines contain clear slickenfibres (Fig. 6f) from which a left-lateral sense of displacement can be deduced. On other slip planes, however, slickenfibres or fibre steps are lacking. Fortunately, also the displacement of prominent clayey paleosol horizons in the Alimoğlu quarry can be used as a clear kinematic marker. Three paleosols (numbered *1* to *3*) are laterally displaced by the activity of faults L3.300, L3.312 and L3.322. The most eastern paleosol *1* is 40 cm to 50 cm thick and is present on level 3 in the central part of the Alimoğlu quarry (Fig. 8a). It laterally extends for 50 m and gently decreases in thickness towards the SE. In the NW of the quarry, paleosol *1* is displaced by fault L3.300 but its prolongation is absent on level 4, either due to lateral thickness decrease or due to fault displacement. The absence of paleosol *1* at the other side of the fault impedes calculating the displacement of fault L3.300. More to the SE, paleosol *1* is cut by fault L3.312 and can be found *c.* 0.3 m higher on the ESE side of fault L3.312 (Fig. 8a). At level 4, the *c.* 0.10 m thick paleosol *2* has been displaced in a similar way. Unfortunately, it disappears in the subsurface before reaching fault L3.322. Further to the ESE, paleosol *3* is present and is cut by fault L3.322. It displaces the horizontally bedded travertine in an apparent vertical direction of 0.30 m (Figs. 6b and 8d). This vertical displacement, however, does not fit with the observed oblique to horizontal slickenlines on the fault slip planes and the left-lateral fibre steps observed on fault L3.300. Therefore, based on the minor lateral displacement of the paleosols along faults L3.312 and L3.322, the oblique slickenlines measured on the slip planes of faults L3.300, L3.312 and L5.501, and the left-lateral fibre steps on fault L3.300, oblique-slip to strike–slip can be proposed as the driving fault mechanism displacing the paleosols. The apparent vertical displacement of the paleosols can thus be explained by sinistral faulting which probably does not exceed 1 m.

Between the different fault blocks, the orientation of the horizontally bedded travertine and the paleosols change from 5° dipping to the ESE to *c.* 10° to the SE. This lateral change indicates that the faults had, apart from a translational, also a small rotational component (Fig. 8d). The blocks between the closely spaced faults thus rotated as rigid bodies as demonstrated by the varying dipping angle of the paleosols in the Alimoğlu quarry. This effect of block rotation is however minor.

### 5.2. Çakmak and İlik quarries

The WNW–ESE oriented Çakmak quarry and the NNE–SSW-oriented İlik quarry (Fig. 9a) form one large excavation that is situated in the southern flank of the domal structure, northeast of the Alimoğlu quarry. The Çakmak quarry (Fig. 10a) is approximately 500 m long and 100 m wide, whereas the İlik quarry (Fig. 10a and b) is a steep quarry of 200 m long and only 50 m wide. Both quarries are currently excavated in 10 levels of which the height of each quarry wall varies between 5 m and 10 m.

#### 5.2.1. Joint orientation and morphology, colour-banded calcite veins

Based on the orientation, the joints present in the Çakmak and İlik quarry can be subdivided in three distinct, mutual abutting joint sets oriented E–W, NE–SW and NW–SE (Fig. 9). In the İlik quarry the E–W joint set is the dominant set, whereas the NE–SW set dominates in the Çakmak quarry (see rose diagrams on Fig. 9). Only a minor part of the NW–SE joints are present in Çakmak. The E–W dominance in the İlik quarry, however, may be biased by the specific quarry orientation rather than to a certain preference for fracturing. A vertical displacement across the joints is mostly absent or negligible due to very small offsets. On the steep eastern wall of the İlik quarry, both joint length and joint morphology can be clearly observed. Joints are usually several tens of metres high and can be traced between the different levels, despite their bifurcating nature along the height (Fig. 10b and c). It is clear that the sedimentary nature of travertine precipitation controls the joint morphology. In the laminar, horizontally bedded facies in the lower levels of the quarries joints propagated freely and were not hampered by any lithological control which resulted in straight fractures. From level 6 onwards short irregular and bifurcating joints are more abundant, often disturbed by the presence of several cavities. Here cascade and waterfall travertine dominate.

The fractures in both quarries are mostly unfilled open extension joints with opening widths up to maximum 5 cm. Joint infill is dominated by brown oxidised clays and by white travertine powder from the current excavation. On levels 1, 2, 3 and 6, joints are sometimes filled with colour-banded calcite precipitation (Fig. 10d, e and f). These banded calcite veins often curve into the laminar porous travertine adjacent to it, forming a horizontally banded vein (Fig. 10d). The coloured bands vary from brown or dark brown to white. Some veins (e.g. joint L2.03; Fig. 10f) can have complex morphologies comprising vertical coloured bands alternating with horizontal to gently inclined calcite and micritic bands. These horizontal bands are surrounded by a white/grey calcite rim dominated by calcite crystals growing internally from the outer wall to the centre (Fig. 10g).

#### 5.2.2. Fault orientation and morphology

In the Çakmak quarry six faults have been identified. Four of them are continuous in the İlik quarry and show a fault length exceeding

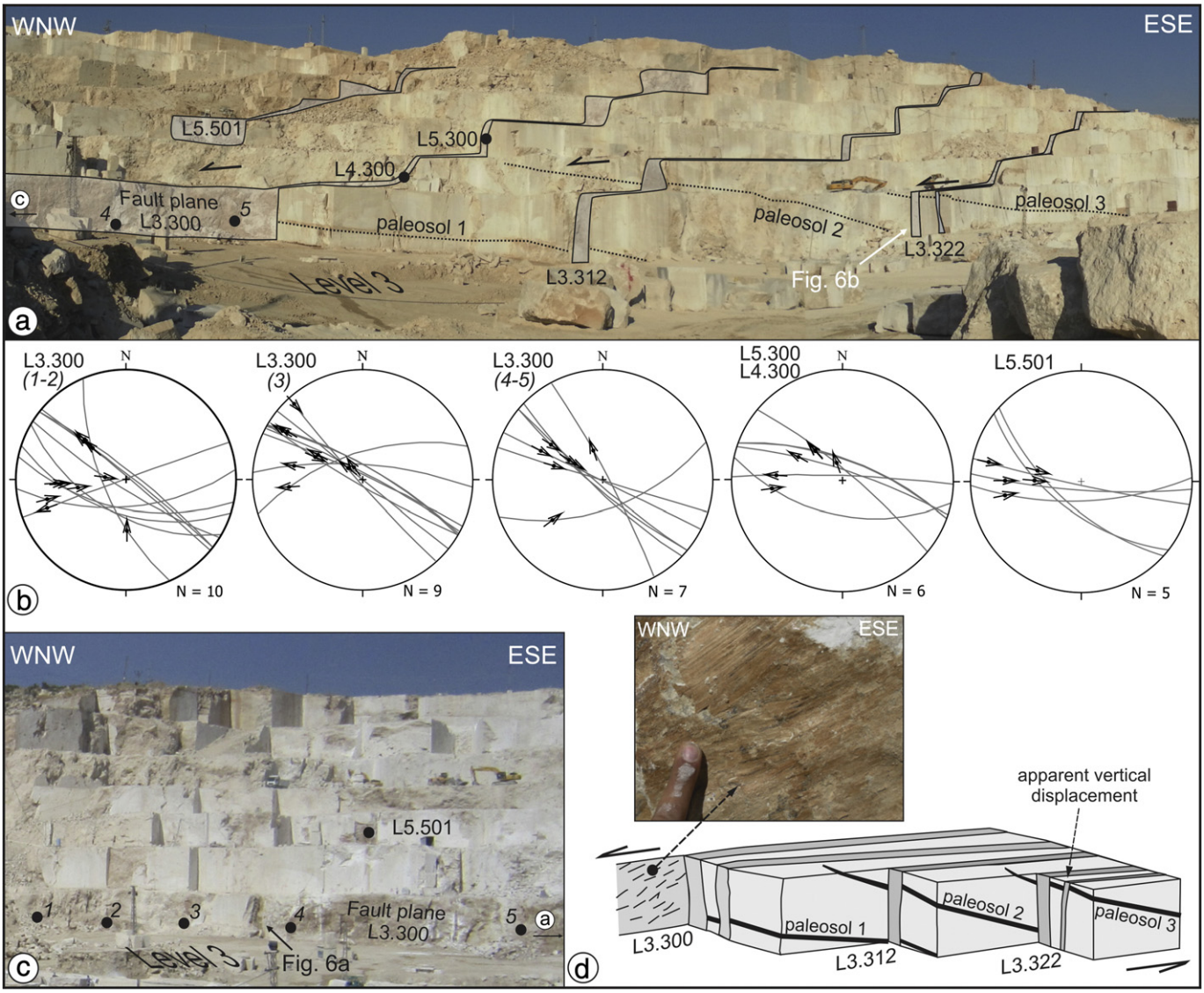


**Fig. 8.** (a) Overview of the central part of the Alimoğlu quarry with indication of four faults transecting the quarry. Block dots are the different observations points. (b) Kinematic analysis of slickenline orientation measured at the different faults illustrated in (a) and (c). Slickenline orientation ranges from NW to W and are gently to moderately plunging. Data in the lower-hemisphere, equal-area stereographic projections demonstrate the kinematics of oblique and strike–slip faults. (c) Eastern part of the Alimoğlu quarry with indication of the fault observation points (black dots). (d) 3D block model showing the sinistral, lateral displacement of the paleosols present on level 3.

300 m (Fig. 9). The most southern observed L1.103 fault in the İlik quarry is the lateral extend of the L7.700 fault in the Alimoğlu quarry (Fig. 4). Orientation of the nearly vertical faults is dominant E–W in the Çakmak quarry and gradually changes to a WNW–ESE orientation in the İlik quarry. Contrary to the Alimoğlu quarry, fault width generally does not exceed 0.5 m and travertine debris blocks are absent. Colour-banded calcite veins with alternating white and brown bands are only observed in fault L4.53. Fault infill is dominated by brown oxidised clays in which often centimetre-size gravel and black organic sediments occur (e.g. in Çakmak faults L4.53, L5.172, L5.28a, L8.290 and in İlik faults L3.209 and L4.209). The gravel consists of variable composition such as marl, limestone, chert and serpentinite. The clastic sequence, i.e. a polymict conglomerate, overlying the travertine in Çakmak and İlik (Fig. 10c) is likely the origin of the gravel. The fact that gravel is found in the faults, even in the lower levels, suggests that the faults acted as open systems during certain periods in which sedimentary infill from above was possible. This is clearly demonstrated in the İlik quarry in which fault L6.610 (=prolongation of L2.53 in Çakmak) cross-cuts the conglomeratic layer at the top of level 9. Remarkably, fault L6.610 cross-cuts the conglomeratic layer on level 9 without any vertical displacement (Fig. 11). Also in the lower levels of Çakmak, displacement across the same fault L2.53 is absent. Hence, it is likely that L2.53 and its continuation L6.610 in İlik is an open extensional fissure of 0.5 m wide rather than a true fault.

In the lower levels of both quarries any lateral or vertical offset along the faults remains undetermined due to the lack of clear marker beds in the horizontally bedded travertine facies. In the higher levels, there is an absence in lateral continuity in lithology because of the rapidly variegated nature of the lithology (reed, cascade and waterfall lithofacies). Near faults it is often unclear whether the changing lithology around opposite fault walls has a lithological or tectonic origin. Only in the İlik quarry, the two opposite fault walls of fault L1.103 display a certain minor displacement. However, a lack of clear marker beds and the absence of kinematic indicators such as slickenlines and striations inhibit deducing the fault displacement and fault kinematics.

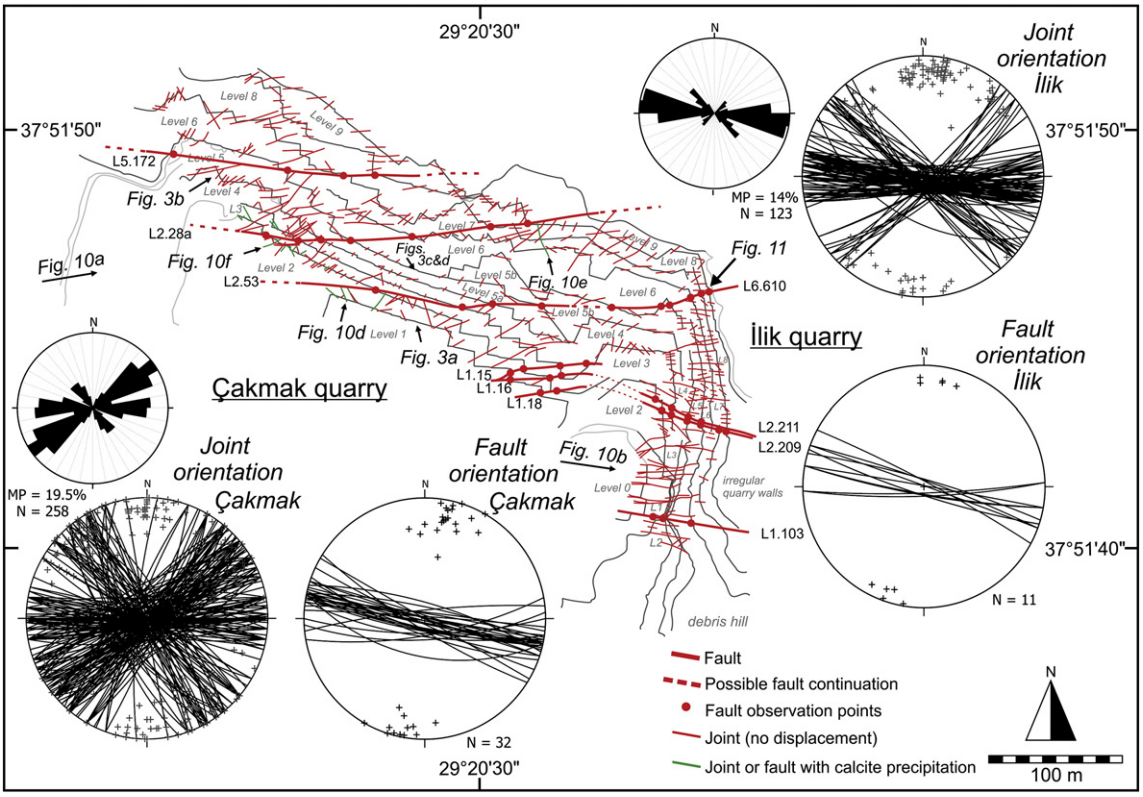


**Fig. 9.** Detailed fault/fracture map of the Çakmak and İlik quarries. Joint and fault orientation are displayed on lower-hemisphere, equal-area stereographic projections. Joints in the centre of the Çakmak quarry are rather absent due to the presence of the cascade and waterfall lithofacies. The rose diagrams display joint orientation and visualise three distinct joint sets in both quarries. The NE–SW set is more represented in the Çakmak quarry, whereas the E–W set occurs more frequently in the İlik quarry. Sector size is 10°. Maximum percentage (MP) marks the perimeter.

### 5.3. Faber and Ece quarries

The Faber quarry is a round open pit with a width of 230 m, the length is approximately 360 m (Fig. 12). The northeastern part of the quarry is more densely fractured (Fig. 13a and b) than the southeastern part. The southeastern quarry wall is *c.* 60 m high and provides a very good view on the vertical (dis)continuity of joints (Fig. 13c and d). The elongated Ece quarry is 400 m long and its width varies between 40 m and 150 m.

#### 5.3.1. Joint orientation and morphology

Due to the absence of any faults in Ece, it was decided to study this quarry in less detail. This explains the rather limited amount of joint measurements in ECE. The joints drawn on the NNE–SSW quarry walls of Ece (Fig. 12) are illustrative for the orientation and density of fracturing. It is most likely that joints in levels 1 and 2 are continuous and can be interconnected showing a joint length of several tens of metres. Joints in the WNW–ESE quarry walls have not been studied in detail and are only illustrated in order to provide an overview of the joint orientation.

Similar to the other quarries, three joint sets with a NE–SW, NW–SE and E–W orientation are deduced in the Faber and Ece quarries. In both quarries the E–W oriented joint set is clearly the dominant set (see stereoplot analysis on Fig. 12). The majoritiy of joints are open, unfilled extensional fractures across which displacement is absent. Calcite precipitation has only been observed in the cavities and presumably relates to speleothem development (cf. Fig. 3e). In the eastern part of the quarry a cluster of fractures occurs in an area of 70 m around the ENE–WSW oriented strike–slip L2.200 fault (see Section 5.3.2.; Figs. 12, 13a and b). The steep, 60 m high excavation wall in the southwestern part of the Faber quarry provides a very good overview on the joint distribution and joint morphology (Fig. 13c and d). Joints are usually steeply dipping and are several tens of metres high, bifurcating along their height. There is no regular joint spacing.

#### 5.3.2. Fault orientation, morphology and kinematics

Two faults have been recognised in the Faber quarry (L2.200 & L2.201). The most southern fault L2.200 is a narrow ENE–WSW trending fault (width <0.5 m) which can be located on all excavation levels. The prolongation of this fault can be observed in a small quarry East of Faber which allows estimating a minimum fault length of 420 m (Fig. 12). The fault plane dips steeply to the south (190/88; Fig. 14a) and is often completely polished due to fault activity (Fig. 14b). The polished surface consists of black and white calcite precipitation which is marked by many ESE–WNW trending slickenlines that are horizontal (280/00) or gently ESE-plunging (116/10; Fig. 14b). Based on the displacement of a paleosol on level 3, a sinistral fault movement can be deduced with a lateral displacement of *c.* 0.5 m. Similar to fault L2.200, fault L2.201 dips steeply to the south (190/80). On the polished surface ENE–WSW trending slickenlines have been observed, oriented either horizontally (280/00) or gently WNW-plunging (279/11) (Fig. 14c). In both faults, the horizontal set overprints the gently plunging set (Fig. 14b and c), indicating that the former is younger than the latter. The superimposition of these kinematic indicators is usual in tectonic regimes in which the faults play for long periods and in which a local stress field can undergo a slight variation through time. Due to the very small variance between both sets of slickenlines, one may determine one stress field orientation out of these kinematic data (see Section 6).

Remarkably, the travertine mass between L2.200 and L2.201 is densely fractured (Fig. 13a and b). This fractured zone has a fracture

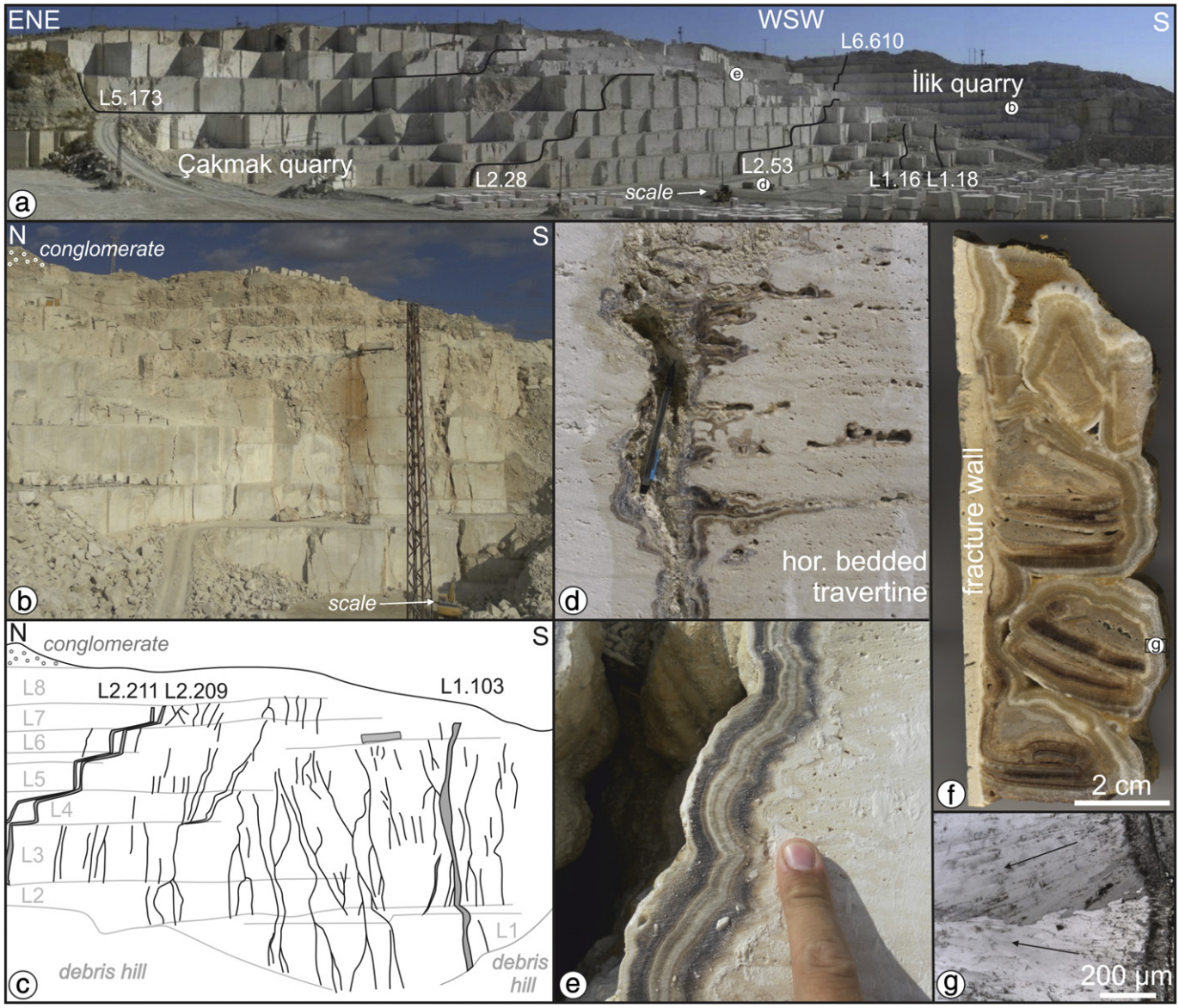


**Fig. 10.** Characteristics of the Çakmak and İlik quarries. See Fig. 9 for picture localisation. (a) Faults in the Çakmak quarry. (b) Photograph and (c) interpretative drawing of fault and joint morphology in the İlik quarry. Joints have a height of several tens of metres high and regularly bifurcate. Faults can be traced between the different levels. (d) Colour-banded calcite in the lower part of the Çakmak quarry (fracture L1.03, level 1) showing the lateral infiltration of precipitating fluids in the horizontal bedded travertine. Pencil (12 cm) for scale. (e) Typical white-brown colour-banded travertine vein developed on the western fracture wall. of joint L6.236. (f) Cut sample of joint L2.35 showing complex vein morphology. The vein developed from the fracture wall to the centre of the fracture. Thin calcite rafts and horizontal precipitation are surrounded by a rim of banded white calcite precipitation. (g) Detail of (f) showing growth competition between the calcite crystals in the surrounding rim.

density which is much higher than elsewhere in the Faber quarry or in the other quarries. Fractures are closely spaced (<0.5 m) and minor normal displacement can sometimes be deduced. Fractures south of the fault L2.200 change in orientation from steeply dipping and parallel to the fault, i.e. E–W to ENE–WSW, to gently dipping with an NW–SE orientation further away from the fault (see grey arrow in stereoplot on Fig. 14d). Although the fault is only 0.5 m wide, this damage zone reaches up to 70 m. Outside the damage zone, joints are long and align in their regional orientation. The morphology of this fracture zone, in particular the changing dip and dip direction of the fractures further away from the fault, indicates that this fracture zone can be interpreted as a typical positive flower structure developed in the footwall of the large left-lateral strike–slip fault L2.200 that cross-cuts the Faber quarry. This is the only known example in the study area in which a clear damage zone has been observed.

### 5.4. Synthesis domal area

Based on numerous measurements it can be concluded that there are three distinct joint orientations. Abutting relationships are changing and it is suggested that the development of the different joint sets may co-occur. The E–W to locally WNW–ESE joint set is dominantly present over the NE–SW and NW–SE joint sets in all quarries. Most joints are open, extensional fractures that bifurcate along their length and height, and across which no displacement can be deduced. They often cross-cut the different travertine facies and can therefore be defined as non-stratabound joints (sensu Gillespie et al., 1999; Van Noten and Sintubin, 2010). Some joints are filled with travertine powder or are mineralised by colour-banded calcite precipitations. These veins can have a complex internal morphology consisting of vertical calcite bands and horizontal mineralisations and rafts.

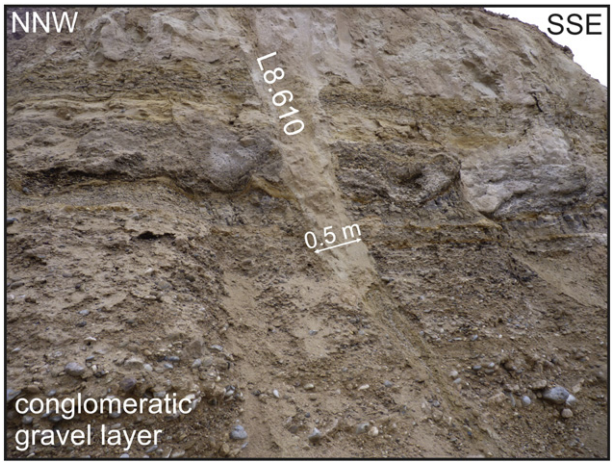


**Fig. 11.** Fault L8.610 (prolongation of L6.610 in the İlik quarry and L2.53 in the Çakmak quarry) cutting through the conglomeratic/gravel level on top of the travertine deposits in the Çakmak and İlik quarries. Absence of any vertical displacement gives rise to a 0.5 m open fissure rather than a fault. See Fig. 9 for picture localisation.

Faults in the domal area have an E–W to WNW–ESE orientation and are continuous between the different quarries reaching several hundred metres in length. Faults are filled with oxidised clays, organic layers, veins, travertine debris and locally with gravel of varying composition originating from an overlying, sometimes unconsolidated, conglomeratic layer. This varying fault infill suggests that these faults acted as open systems, or sometimes just as large open fissures, that may have reached the surface during rupturing. With the exception of fault L2.200 in the Faber quarry, all faults developed without significant wallrock deformation or fault rock development. Only six faults bear kinematic evidences that allow the deduction of the displacement along the faults. In the Alimoğlu quarry faults L3.300 and L5.501 contain several striated surfaces. The displaced paleosols between faults L3.300, L3.312 and L3.322 suggests an oblique, sinistral fault displacement between these faults. Based on the striated fault planes of the L2.200 and L2.201 faults in the Faber quarry, a strike–slip, sinistral fault movement has been determined.

## 6. Paleostress reconstruction

Principal stress orientations active during faulting can be derived from fault slip data along representative fault planes. Numerous paleostress inversion techniques have been developed in the past. Most of them apply the Wallace–Bott hypothesis (Bott, 1959; Wallace, 1951) stating that slip occurs parallel to the resolved shear stress on a pre-existing or newly formed fault plane. These inversion techniques involve the concept of deriving the best-fitting stress tensor, capable of explaining the direction of slip on the studied faults and the magnitude of the principal stress directions. Due to the limited presence of slickenlines and other kinematic markers only the fault slip data of the L3.300 (n = 32; Fig. 8b) and L5.501 (n = 5) faults in the Alimoğlu quarry and the L2.200 and L2.201 faults (n = 11) in the Faber quarry are used in this paleostress analysis. As explained in the methodology, the graphical Right Dihedral Method (Angelier and Mechler, 1977) optimised in the Win-Tensor program (Delvaux and Sperner, 2003) has been used to calculate the paleostress direction and the magnitude of the stress tensor.

Some of the striations on the L3.300, L4.300 and L5.300 fault plane contain clear left-lateral fibre steps. In cases in which fibre steps are lacking, the sinistral displacement of paleosols *2* and *3* is used as the direction of displacement on the striations in the stereoplots on Fig. 15. Deriving a single stress state out of the L3.300, L4.300 and

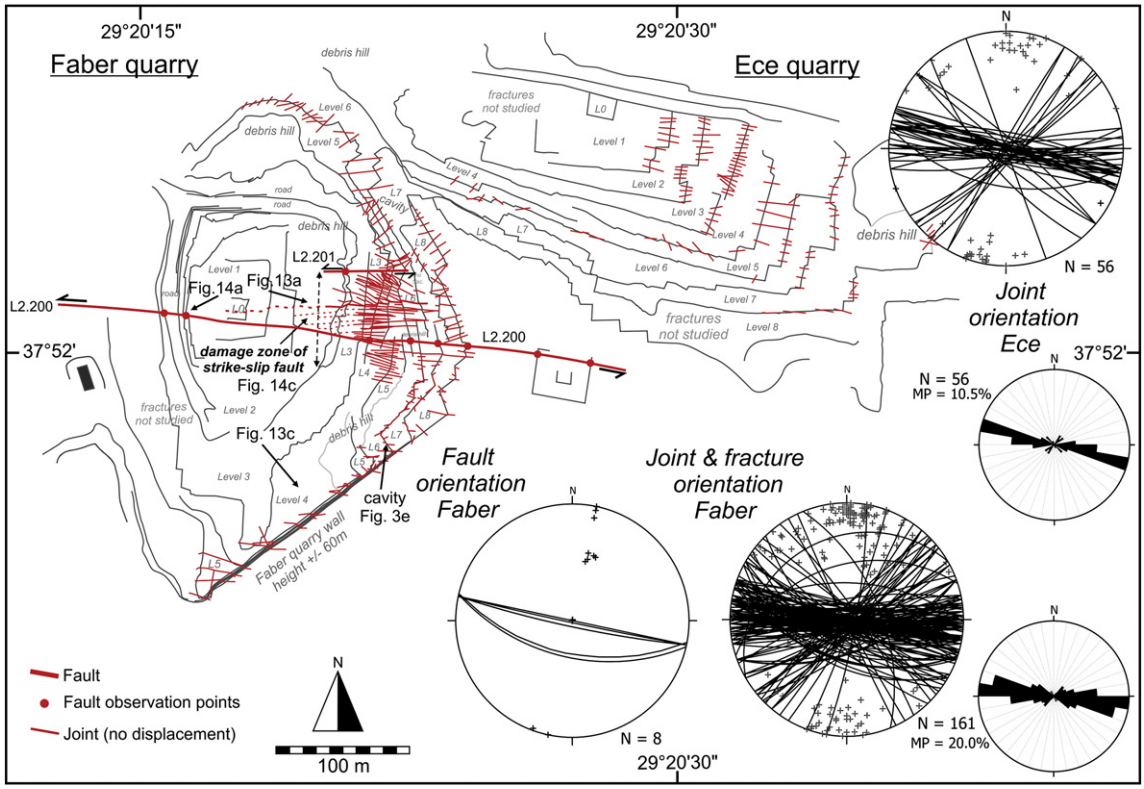


**Fig. 12.** Detailed fault/racture map of the Faber and Ece quarries. Joint, fracture and fault orientation are displayed on lower-hemisphere, equal-area stereographic projections. The Faber quarry is characterised by two steeply S-dipping, left-lateral strike–slip faults. Between both faults, the travertine mass is densely fractured. Faults are absent in the Ece quarry. Only those joints that are measured in the Ece quarry are drawn. The rose diagrams display joint orientation and visualise one distinct fault-parallel joint set. Sector size is 10°. Maximum percentage (MP) marks the perimeter.

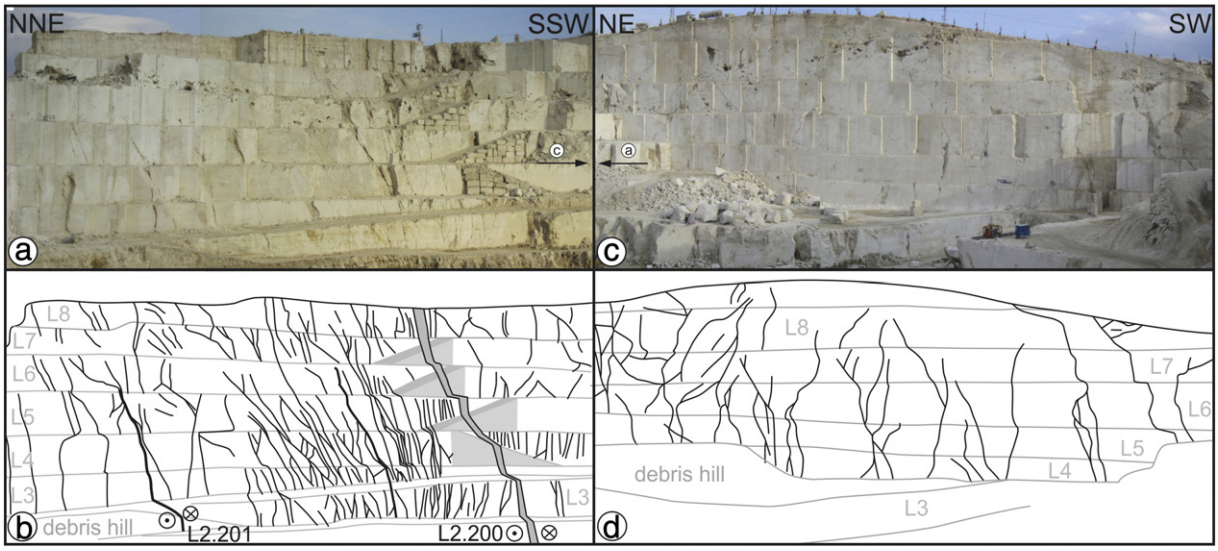


**Fig. 13.** Joint and fracture morphology in the Faber quarry. See Fig. 12 for picture localisation. (a) Photograph and (b) interpretative drawing of the northeastern part of the Faber quarry. The northern footwall of the L2.200 strike–slip fault is more densely fractured compared to its southern hanging wall. Width of picture 200 m. (c) Photograph and (d) interpretative drawing of the steep excavation wall in the southeastern part of the Faber quarry showing bifurcating joints. Width of picture is 100 m.

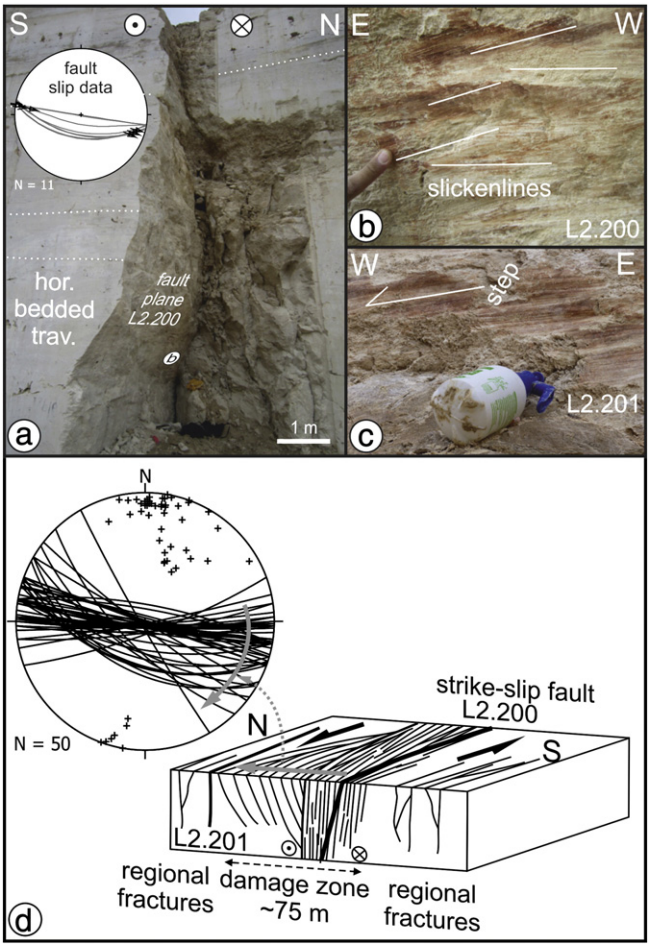


**Fig. 14.** Fault characteristics of the Faber quarry. See Fig. 12 for picture localisation. (a) Steeply south-dipping, E–W oriented, left-lateral strike–slip fault in the Faber quarry (fault L2.200, level 2) and detail of the observed slickenline orientations. (b) Horizontal slickenlines overprint the gently plunging slickenlines. Fingernail (1 cm) for scale. (c) Nearly horizontal slickenlines on the polished surfaces of fault L2.201. (d) Interpretative block diagram of the damage zone of the left-lateral strike–slip fault in the Faber quarry. The grey arrow illustrates the changing fracture orientation in the damage zone. Fractures are steeply dipping and fault-parallel close to fault and change in orientation to SSW-dipping further away from the fault. Block diagram is 125 m wide.

L5.300 Alimoğlu fault data (Fig. 8b) is not possible due to the complexity of the data. To overcome this problem, the Win-Tensor program separated the fault slip data in two different sets (Fig. 15). The first set (n = 18) contains all WNW-plunging oblique slip data, whereas all gently plunging striations are grouped in the second set (n = 10). Only 4 measurements have been rejected by the program and consequently they are not used in this analysis. Inversion of the first set results in a sub-vertical $\sigma_1$ (237/52) and sub-horizontal $\sigma_2$ (113/28) and $\sigma_3$ (351/25). This specific stress state is indicative of extension in a NNW–SSE direction. Inversion of the second set, however, points towards a vertical $\sigma_2$ (092/77) and horizontal $\sigma_1$ (231/10) and $\sigma_3$ (322/08), indicative of a strike–slip regime with a NE–SW oriented $\sigma_1$ (Fig. 15). Inversion of the L5.501 fault in the Alimoğlu quarry results into a sub-vertical $\sigma_2$ (124/78) and horizontal $\sigma_1$ (228/02) and $\sigma_3$ (327/12), indicative of a similar NE–SW oriented strike–slip stress regime as the L3.300 fault (Fig. 15).

A few fibre steps and the displacement of an erosional level indicate a sinistral displacement along the L.200 and L2.201 faults in the Faber quarry. Inversion of these fault data results into a sub-vertical $\sigma_2$ (201/68) and horizontal $\sigma_1$ (059/17) and $\sigma_3$ (235/12), evidencing a similar NE–SW oriented strike–slip regime as the Alimoğlu faults (Fig. 15).

## 7. Discussion

### 7.1. Speleothems and banded calcite veins

In the quarries in the study area several different calcite veins have been observed. Based on macroscopic features, they can be separated into speleothems and banded calcite veins.

The speleothems occur as columnar colour-banded calcite and result from the descent of surficial waters in cavities (Fig. 3e) and along fault walls (Fig. 7b and c; fault L3.312 in the Abandoned quarry). In the latter example, the presence of speleothems emphasises the open nature of the faults. The horizontal calcite rafts in the cavities originate from precipitation in stagnant waters.

The complex colour-banded calcite veins, which are only observed in some joints and faults, represent fluctuations in calcite precipitation. The combined vein morphology of vertical and horizontal bands of calcite precipitation (Fig. 10d, e and f) likely originate from a complex multiphase joint infill either from a hydrothermal or a meteoric source. Remarkably most calcite veins are found at lower levels

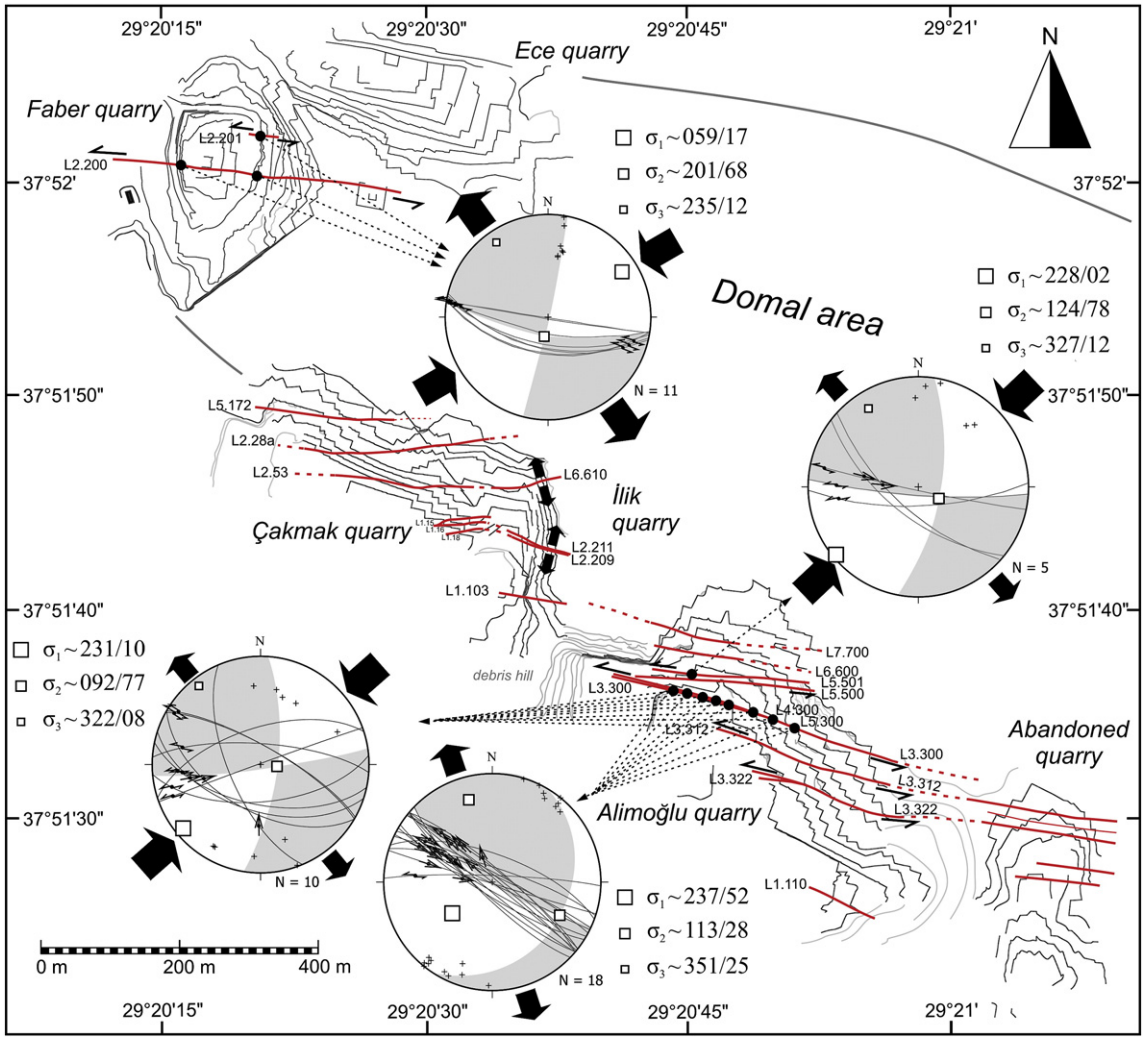


**Fig. 15.** Overview of faults in the studied quarries in the domal area. The four lower-hemisphere, equal-area stereographic projections show the results of a paleostress analysis. This analysis is performed on slickenline orientations observed (black dots) on the fault planes of the L3.300 (also on level 4 and 5) and L5.501 faults in the Alimoğlu quarry and the L2.200 and L2.201 faults in the Faber quarry. The grey beachball in each stereograph illustrates the average fault plane solution calculated by paleostress inversion. Inversion of the Alimoğlu fault data results into NNW–SSE oriented extension (roughly N–S extension) and NE–SW oriented left-lateral strike–slip. Inversion of the Faber fault data results into similar NE–SW oriented left-lateral strike–slip. Two faults in Çakmak are indicative of NNW–SSE and NNE–SSW extension.

(e.g. Level 2, Çakmak quarry) and show absence of any continuity towards upper levels. The calcite veins are also mostly absent in larger faults indicating that, after travertine development, secondary fluid flow was restricted and migrated through the pore- and fracture network, rather than it was related to large-scale faulting. The origin of the precipitating waters is currently the subject of ongoing and unpublished research which focuses on stable $\delta^{13}C$–$\delta^{18}O$ isotope analysis of the joint infill and microthermometry of fluid inclusions in the calcites. Similar geochemical studies on travertine veins have demonstrated that such analyses are successful to determine the source of precipitating fluids (e.g. Çolak et al., 2011; De Filippis et al., 2012; Kele et al., 2011; Uysal et al., 2009).

### 7.2. Paleostress states deduced from the joint network

Neotectonic joints occur pervasively in shallow tectonic environments, especially in undeformed basins and platforms (Dunne and Hancock, 1994). The alignment and the consistency in orientation of joints and extension veins have numerously been used to determine the orientation of a paleostress field at the time of fracturing (e.g. Dewit et al., 2012; Gillespie et al., 1999; Jacquemyn et al., 2012; Kaymakçı, 2006; Van Noten et al., 2011, 2012; Verhaert et al., 2006). In this respect, extension (mode I) fractures, i.e. joints, and extension veins open perpendicular to the minimum principal stress ($\sigma_3$) and propagate in the plane of the maximum ($\sigma_1$) and intermediate ($\sigma_2$) principal stress (Secor, 1965).

The lack of striations on the observed fractures and the mutual abutting joint sets makes it difficult to work out a time history for the different joint sets in the study area. Nevertheless, based on their orientation some assumptions can be made and tentative evolution of joint development can be composed, taking into account the limitations of using joint sets as paleostress markers (Dunne and Hancock, 1994). Bearing in mind that all joints are (sub)vertical, a compressional stress regime as corresponding regime can be rejected as joints in such a regime should be oriented horizontally. Throughout the different quarries, the E–W joint set is the most dominant set. Such a joint set would either correspond to a N–S extensional regime or an E–W oriented strike–slip regime. Given the fact that conjugate shear fractures are not observed (all fractures are individual or bifurcating joints) and taking into the account the regional N–S extensional framework in the eastern part of the Denizli Basin, a strike–slip regime can be rejected and an extensional stress regime

is most likely. The E–W joint set can thus kinematically be linked to N–S extension that gave rise to the current shape of the eastern part of the Denizli Basin. In this respect, joint formation is either related to regional stress or to the reflection of deformation related to the (blind) normal faults in and below the travertine mass, a deformation pattern typical in the Aegean region (Stewart and Hancock, 1990).

Relating joint sets from a restricted outcrop area to regional fault data without anchorage to main faults may be speculative, however, also in the NW-trending part of the Denizli Basin, i.e. in the Pamukkale fault zone, numerous NW–SE trending tension fractures have been demonstrated to correspond to the NE–SW extension that has affected this region and acted during or after travertine accumulation (Altunel and Hancock, 1993a; Altunel and Karabacak, 2005; Kaymakçı, 2006). Relating the joint orientation to local stress directions in our study area may therefore be valid.

As mutual abutting relationships have been observed, there is no clear timing relationship between the E–W joint set and the NW–SE and NE–SW joint sets. This supports the idea that joint development of the three sets co-occurred. Similar to the E–W joint set, there is no evidence of shearing along the NE–SW and NW–SE joints. Also, given the nearly orthogonal angle between the orientation of the NE–SW and NW–SE joint sets a conjugate fracture system can be excluded, especially because the superimposition of different brittle structures does not give rise to geometrical patterns as expected for undeformed material. It may thus be plausible that the NE–SW and NW–SE joints correspond to NW–SE and NE–SW extension respectively.

The high seismicity that has been recorded the last centuries shows that extension in the Denizli Basin is still active and predominantly occurs along normal faults (Kaypak and Gökkaya, 2012). The most recent earthquake in the E–W trending part of the Denizli Basin occurred on April 25, 2008 and had a magnitude of Mw = 4.9. Its epicentre was located at about 2 km north of Kocabaş and its focal mechanism was indicative of a SW-dipping NW–SE normal fault with a minor left-lateral strike–slip component (data from EMSC, 2012; Irmak and Taymaz, 2009). Fault plane solutions calculated from other recent earthquakes in the Denizli Basin show that current extension dominantly occurs in a NE–SW direction and in a NW–SE direction in the adjacent Baklan Graben (Irmak and Taymaz, 2009; Kaypak and Gökkaya, 2012; Price and Scott, 1994; Taymaz and Price, 1992; Westaway, 1993). So given the current NE–SW extension in the NW–SE and E–W trending parts of the Denizli Basin and NW–SE extension in the adjacent Baklan Graben, it is likely that during the late Pleistocene and Holocene NE–SW as well as E–W and NW–SE extension could have affected the travertine mass.

The occurrence of both NW–SE and E–W joints in travertine ridges in the NW–SE trending part of the Denizli Basin has lead Altunel and Hancock (1993a) to conclude that N–S extension in the adjacent Büyük Menderes Graben locally influenced NE–SW extension in the Denizli Basin. At Kocabaş, Özkul et al. (2002) and Altunel and Karabacak (2005) reported the presence of E–W and NW–SE trending travertine fissure ridges that are indicative of respectively N–S and NE–SW extension in the E–W part of the Denizli Basin. Moreover, also Kaymakçı (2006) and Taymaz and Price (1992) demonstrated that in this area both NE–SW and NW–SE extension has been active and that stress permutations are amplified due to the interference of the Denizli and adjacent Baklan Graben. In addition, also in the Burdur-Isparta region, paleostress analysis on joints and faults have indicated that Quaternary NE–SW and NW–SE stress transitions have occurred and that they are related to the influence of crossing graben structures (Verhaert et al., 2004, 2006).

In the West Anatolian Extensional Province transient stress permutations are thus common (Altunel and Karabacak, 2005; Cihan et al., 2003; Kaymakçı, 2006; Verhaert et al., 2006). As close to the Earth's surface differential stress is low (Hancock and Engelder, 1989), the difference in magnitude between $\sigma_2$ and $\sigma_3$ will be small. Therefore, $\sigma_2$ and $\sigma_3$ can switch temporarily due to small stress changes. Nevertheless the regional limitations of our measurements, stress permutations occurring in the Quaternary can be proposed as the mechanism for the presence of different joint sets in the E–W trending part of the Denizli Basin. Hence the E–W, NE–SW and NW–SE joint sets reflect the local influence of respectively N–S, NW–SE and NE–SW extension along nearby (blind) faults.

### 7.3. Paleostress states deduced from fault data

According to Anderson's (1951) principle, stresses in the Earth are oriented either vertical or horizontal. For the derived strike–slip regimes of the different faults, the deviation of $\sigma_2$ with respect to the vertical remains rather small. Inversion analysis of the first set of the Alimoğlu L3.300 fault, however, has deduced the presence of an extensional regime with oblique stress axes. Theoretically, paleostress axes of newly formed faults cannot have oblique stress axes (Angelier, 1994). The fact that the resulting principal stress axes of the first set are oblique thus indicates that both fault reactivation and block rotation of a non-oblique fault system has occurred in the Quaternary (Angelier, 1994). This can be explained as follows. The mapped faults in the travertine body are situated in the E–W trending part of the Denizli Basin and have E–W to ENE–WSW orientations. The initiation of these steep E–W trending faults is related to N–S extension. Clear markers of the N–S extension are the numerous E–W joints and the two L2.28a and L2.53 faults in the Çakmak quarry (and their prolongation L6.610 in the İlik quarry) along which no displacement has been observed (Fig. 15). Evidence of N–S normal faulting is also present in the travertine quarries in the northern graben edge (Özkul et al., 2002). Additionally, Westaway (1993) demonstrated that several normal faults in the Denizli Basin have unusual steep dips of more than 80°, which is in agreement to our observations.

The displaced paleosols and the minor change in the orientation of travertine bedding between the L3.300, L3.312 and L3.321 faults in the Alimoğlu quarry evidence that strike–slip faulting as well as minor block rotation have been superimposed on some normal faults in the Alimoğlu quarry. Consequently, after the initiation of the steep normal faults a change in the local stress field must have occurred in order to reactivate some normal faults into left-lateral strike–slip deformation. This thus explains the oblique stress axes derived in the first set of the Alimoğlu L3.300 fault in the paleostress analysis. Price and Scott (1994) demonstrated that block rotation is common along basin-bounding faults of the Denizli Basin and Baklan Graben and thus possibly also caused tilting of the travertine body.

The flower deformation structure and the absence of any evidence of normal faulting in the Faber quarry suggest that the L2.200 and L2.201 faults likely developed during the strike–slip regime. In general, the strike–slip deformation can be interpreted as a counterclockwise rotation around a sub-horizontal axis which led to a transpressional reactivation of the E–W to ENE–WSW trending faults in the travertine body or has led to newly formed faults (Faber).

In many cases in the Denizli Basin, for example in the step-over fault zones in the Pamukkale fault zone and further northwest, dominant dip-slip normal faults are observed that contain subordinate components of strike–slip (Altunel and Hancock, 1993a,b; Bozkurt and Sözbilir, 2006; Çakır, 1999; Koçyiğit, 2005). Also Gürbüz et al. (2012) demonstrated the presence of oblique-slip and left-lateral strike–slip along the NE–SW oriented basin-bounding Baklan and Çal faults in the adjacent Baklan Graben. They proposed that these lateral movements must have taken place on the boundaries of inner horsts and grabens. Furthermore, in the Dinar-Baklan region in the SE a counterclockwise rotation occurred because of differential stretching along the inner blocks in the Baklan and Acıgöl Grabens on top of the NW-trending Dinar Fault (Gürbüz et al., 2012), which is considered as a listric breakaway fault (Sintubin et al., 2003; Westaway, 1993). Currently it is unknown what has caused the reactivation of the faults in the study area but possibly fault activity

in the adjacent Baklan Graben may have interfered with overall extension in the local E–W trending part of the Denizli Basin (cf. Kaymakçı, 2006) which could have resulted into the observed strike–slip deformation.

### 7.4. Timing relationships

A paleostress reconstruction of the different brittle stages after travertine deposition leads to the following tentative stress field evolution. Considering the similar geometry of the E–W oriented joints and faults, a chronological order between joint- and fault formation cannot be constructed at this stage of research. Joints possibly initiated together with the development of E–W normal faults in the northern graben edge of the Denizli Basin. Concomitant with E–W jointing, stress permutations related to nearby fault activity caused the formation of NE–SW and NW–SE joint sets. Except for the intensification of fracture density towards to L2.200 fault in the Faber quarry, there is no geometrical relationship between joint formation and strike–slip reactivation of the normal faults. It is therefore proposed that a transient strike–slip regime with a NE–SW maximum stress tensor postdates the development of the joint network. Earthquake fault plane solutions show that the southwestern part of the Denizli Basin currently is in NE–SW extension.

## 8. Conclusions

This study has analysed a large set of neotectonic brittle structures that have deformed a km-scale travertine body situated at the graben intersection of the locally E–W oriented Denizli Basin and the NE–SW oriented Baklan Graben, SW Turkey. The dense joint network observed in the Alimoğlu, Çakmak, İlik, Faber and Ece quarries reflects brittle extensional fracturing caused by local extension in the SW part of the Denizli Basin. The dominant E–W joint set can be related to local N–S extension. The two other mutually abutting NW–SE and NE–SW joint sets correspond to respectively NE–SW and NW–SE extension. These three mutual abutting joint sets are indicative of stress permutations between $\sigma_2$ and $\sigma_3$ in a remote extensional stress regime, caused by the temporarily interaction of activity along faults in the NW–SE part of the Denizli Basin and in the Baklan Graben. The presence of colour-banded calcite veins present in some joints reflect multiphased calcite precipitation resulting from fluid flow of unknown origin.

Several E–W- to locally ENE–WSW trending faults cross-cut the studied travertine body. The faults are filled with organic layers and oxidised travertine powder of human activity. In the Çakmak quarry, fault infill often contains siliciclastic gravel that originates from an overlying conglomeratic level above the travertine body, an observation indicative of the open nature of the faults after faulting. Also the speleothems observed at some fault walls corroborates to this idea. Based on a paleostress analysis of some faults in the Alimoğlu quarry and based on their overall significant E–W to WNW–ESE orientation, faults probably initiated as normal faults in the E–W trending part of the Denizli Basin in a remote extensional stress field. A paleostress analysis on kinematic markers such as slickenlines and displaced paleosols allowed determining fault displacements that are superimposed on the pre-existing normal faults. Inversion analysis indicates that, after joint formation, some of the normal faults were reactivated as left-lateral strike–slip faults in a transient strike–slip regime with a NE–SW maximum stress tensor. Fault plane solutions of recent earthquakes show that, similar to its main part, the SW part of the Denizli Basin is currently under NE–SW extension.

## Acknowledgements

The authors would like to acknowledge the quarry owners of the Çakmak, İlik, Alimoğlu, Faber and Ece quarries for their willingness to cooperate and their hospitality during field work. LIDAR scanning of the different quarries was performed by the Geospatial Research Ltd. (Durham University). We are very grateful to Mehmet Oruç Baykara who kindly provided all the logistic help, to Benjamin Lopez and Wim Vandewijngaerde for field assistance and to Carl Jacquemyn for his help with the GPS measurements. Reviewers Andrea Brogi and Andrea Billi are thanked for their comments and for sharing their knowledge on travertine deposits. Fabrizio Storti edited the manuscript. This work was undertaken during a postdoctoral project of Koen Van Noten which frames in a Joint Industry Project (JIP) focusing on the architecture of travertine geobodies. Financial support was provided by Eni, Petrobras, Total and KULeuven R&D.

## References

Aktar, M., Karabulut, H., Özalaybey, S., Childs, D., 2007. A conjugate strike–slip fault system within the extensional tectonics of Western Turkey. Geophysical Journal International 171, 1363–1375.

Alçiçek, H., Varol, B., Özkul, M., 2007. Sedimentary facies, depositional environments and palaeogeographic evolution of the Neogene Denizli Basin, SW Anatolia, Turkey. Sedimentary Geology 202, 596–637.

Altunel, E., Hancock, P.L., 1993a. Active fissuring and faulting in Quaternary travertines at Pamukkale, western Turkey. Zeitschrift fuer Geomorphologie NF 94, 285–302.

Altunel, E., Hancock, P.L., 1993b. Morphology and structural setting of Quaternary travertines at Pamukkale, western Turkey. Geological Journal 28, 335–346.

Altunel, E., Hancock, P.L., 1996. Structural attributes of travertine-filled extensional fissures in the Pamukkale Plateau, Western Turkey. International Geology Review 38, 768–777.

Altunel, E., Karabacak, V., 2005. Determination of horizontal extension from fissure-ridge travertines: a case study from the Denizli Basin, southwestern Turkey. Geodinamica Acta 18, 333–342.

Anderson, E.M., 1951. The dynamics of faulting and dyke formation with application to Britain. Oliver and Boyd, Edinburgh. (206 pp.).

Angelier, J., 1994. Fault slip analysis and paleostress reconstruction. In: Hancock, P.L. (Ed.), Continental Deformation. Pergamin, Oxford, pp. 53–100.

Angelier, J., Mechler, P., 1977. Sur une méthode graphique de recherche des contraintes principales également utilisable en tectonique et en séismologie: la méthode des dièdres droits. Bulletin de la Société Géologique de France 7 (19), 1309–1318.

Bott, M.P.H., 1959. The mechanics of oblique-slip faulting. Geological Magazine 96, 109–117.

Bozkurt, E., 2001. Neotectonics of Turkey – a synthesis. Geodinamica Acta 14, 3–30.

Bozkurt, E., Sözbilir, H., 2006. Evolution of the large-scale active Manisa Fault, Southwest Turkey: implications on fault development and regional tectonics. Geodinamica Acta 19, 427–453.

Brogi, A., 2004. Faults linkage, damage rocks and hydrothermal fluid circulation: Tectonic interpretation of the Rapolano Terme travertines (southern Tuscany, Italy) in the context of Northern Apennines Neogene–Quaternary extension. Eclogae Geoligicae Helvetiae 97, 307–320.

Brogi, A., Capezzuoli, E., 2009. Travertine deposition and faulting: the fault-related travertine fissure-ridge at Terme S. Giovanni, Rapolano Terme (Italy). International Journal of Earth Sciences 98, 931–947.

Brogi, A., Capezzuoli, E., Aqué, R., Branca, M., Voltarrio, M., 2010. Studying travertine for neotectonic investigations: Middle-Late Pleistocene syn-tectonic travertine deposition at Serra di Rapolano (Northern Apennines, Italy). International Journal of Earth Sciences 99, 1383–1398.

Brogi, A., Capezzuoli, E., Buracchi, E., Branca, M., 2012. Tectonic control on travertine and calcareous tufa deposition in a low-temperature geothermal system (Sarteano, Central Italy). Journal of the Geological Society 169, 461–476.

Çakır, Z., 1999. Along-strike discontinuities of active normal faults and its influence on Quaternary travertine deposition; examples from western Turkey. Turkish Journal of Earth Sciences 8, 67–80.

Cihan, M., G., S., Gökçe, D., 2003. Insights into biaxial extensional tectonics: an example from the Sandıkı Graben, West Anatolia, Turkey. Geological Journal 38, 47–66.

Çobanoğlu, I., Çelik, S.B., 2012. Determination of strength parameters and quality assessment of Denizli travertines (SW Turkey). Engineering Geology 129–130, 38–47.

Çolak, S., Özkul, M., Aksoy, E., 2011. Structural, depositional studies on travertine occurrences along strike–slip fault: a case study from East Anatolian Fault System (EAFS), Elazığ, Turkey. Rendiconti Online Società Geoligica Italia 16, 12–13.

De Filippis, L., Billi, A., 2012. Morphotectonics of fissure ridge travertines from geothermal areas of Mammoth Hot Springs (Wyoming) and Bridgeport (California). Tectonophysics 548–549, 34–48.

De Filippis, L., Faccenna, C., Billi, A., Anzalone, E., Brilli, M., Özkul, M., Soligo, M., Tuccimei, P., Villa, I.M., 2012. Growth of fissure ridge travertines from geothermal springs of Denizli Basin, western Turkey. Geological Society of America Bulletin 124, 1629–1645.

Delvaux, D., Sperner, B., 2003. Stress tensor inversion from fault kinematic indicators and focal mechanism data: the TENSOR program. In: Nieuwland, D. (Ed.), New Insights into Structural Interpretation and Modelling: Geological Society, London, Special Publications, 212, pp. 75–100.

Demircioğlu, D., Ecevitoğlu, B., Seyitoğlu, G., 2010. Evidence of a rolling hinge mechanism in the seismic records of the hydrocarbon-bearing Alaşehir Graben, western Turkey. Petroleum Geoscience 16, 155–160.
Dewit, J., Huysmans, M., Muchez, Ph., Hunt, D.W., Thurmond, J.B., Verges, J., Saura, E., Fernandez, N., Romaire, I., Esestime, P., Swennen, R., 2012. Reservoir characteristics of fault-controlled hydrothermal dolomite bodies: Ramales Platform case study, in: Garland, J., Neilson, J.E., Laubach, S.E., Whidden, K.J. (Eds.), Advances in Carbonate Exploration and Reservoir Analysis. Geological Society, London. Special Publications 370, 83–109.
Doutsos, T., Kokkalas, S., 2001. Stress and deformation patterns in the Aegean region. Journal of Structural Geology 23, 455–472.
Dunne, W.M., Hancock, P.L., 1994. Palaeostress Analysis of Small-Scale Brittle Structures. In: Hancock, P.L. (Ed.), Continental Deformation. Pergamin, Oxford, pp. 101–120.
EMSC, 2012. European-Mediterranean Seismological Centre. http://www.emsc-csem.org.
Erten, H., Sen, S., Özkul, M., 2005. Pleistocene mammals from travertine deposits of the Denizli Basin (SW Turkey). Annales de Paleontologie 91, 267–278.
Faccenna, C., 1994. Structural and hydrogeological features of Pleistocene shear zones in the area of Rome (Central Italy). Annali di Geoficia 37, 121–133.
Faccenna, C., Soligo, M., Billi, A., De Filippis, L., Funiciello, R., Rossetti, C., Tuccimei, P., 2008. Late Pleistocene depositional cycles of the Lapis Tiburtinus travertine (Tivoli, Central Italy): possible influence of climate and fault activity. Global and Planetary Change 63, 299–308.
Gillespie, P.A., Johnston, J.D., Loriga, M.A., McCaffrey, K.J.W., Walsh, J.J., Watterson, J., 1999. Influence of layering on vein systematics in line samples. In: McCaffrey, K.J.W., Lonergan, L., Wilkinson, J.J. (Eds.), Fractures, Fluid Flow and Mineralisation: Geological Society, London, Special Publications, 155, pp. 35–56.
Guo, L., Riding, R., 1998. Hot-spring travertine facies and sequences, Late Pleistocene, Rapolano Terme, Italy. Sedimentology 45, 163–180.
Gürbüz, A., Boyraz, S., Ismael, M.T., 2012. Plio-Quaternary development of the Baklan–Dinar Graben: implications for cross-graben formation in SW Turkey. International Geology Review 54, 33–50.
Hancock, P.L., Engelder, T., 1989. Neotectonic joints. Geological Society of America Bulletin 101, 1197–1208.
Hancock, P.L., Chalmers, R.M.L., Altunel, E., Çakir, Z., 1999. Travitonics: using travertines in active fault studies. Journal of Structural Geology 21, 903–916.
Irmak, S., Taymaz, T., 2009. Source Mechanics of Recent Moderate Earthquakes Occurred in Honaz-Denizli (W Turkey) Graben Obtained by Regional Broadband Waveform Inversion. International Symposium on Historical Earthquakes and Conservation of Monuments in the Eastern Mediterranean Region, Istanbul, Turkey, pp. 350–356.
Jacquemyn, C., Swennen, R., Ronchi, P., 2012. Mechanical stratigraphy and (palaeo-) karstification of the Murge area (Apulia, southern Italy), in: Garland, J., Neilson, J.E., Laubach, S.E., Whidden, K.J. (Eds.), Advances in Carbonate Exploration and Reservoir Analysis. Geological Society, London. Special Publications 370, 169–186.
Jones, B., Renaut, R.W., 2010. Chapter 4. Calcareous Spring Deposits in Continental Settings. In: Alonso-Zarza, A.M., Tanner, L.H. (Eds.), Developments in Sedimentology. Elsevier, pp. 177–224.
Kappelman, J., Alçiçek, M.C., Kazancı, N., Schultz, M., Özkul, M., Şevket, Ş., 2008. Brief communication: first *Homo erectus* from Turkey and implications for migrations into temperate Eurasia. American Journal of Physical Anthropology 135, 110–116.
Kaymakçı, N., 2006. Kinematic development and paleostress analysis of Denizli Basin (W Turkey): implications of spatial variation of relative paleostress magnitudes and orientations. Journal of Asian Earth Sciences 27, 207–222.
Kaypak, B., Gökkaya, G., 2012. 3-D imaging of the upper crust beneath the Denizli geothermal region by local earthquake tomography, western Turkey. Journal of Volcanology and Geothermal Research 211–212, 47–60.
Kele, S., Özkul, M., Fórizs, I., Gökgöz, A., Baykara, M.O., Alçiçek, M.C., Németh, T., 2011. Stable isotope geochemical study of Pamukkale travertines: new evidences of low-temperature non-equilibrium calcite-water fractionation. Sedimentary Geology 238, 191–212.
Koçyiğit, A., 2005. The Denizli graben-horst system and the eastern limit of western Anatolian continental extension: basin fill, structure, deformational mode, throw amount and episodic evolutionary history, SW Turkey. Geodinamica Acta 18, 167–208.
Koçyiğit, A., Deveci, S., 2007. A N–S-trending active extensional structure, the Şiuhut (Afyon) graben: commencement age of the extensional Neotectonic period in the Isparta Angle, SW Turkey. Turkish Journal of Earth Sciences 16, 391–416.
Mesci, B.L., Gursoy, H., Tatar, O., 2008. The evolution of Travertine masses in the Sivas area (Central Turkey) and their relationships to active tectonics. Turkish Journal of Earth Sciences 17, 219–240.
Özer, H.M., 2000. Hydrogeology and geochemistry in the Curuksu (Denizli) hydrothermal field, western Turkey. Environmental Geology 39, 1169–1180.
Özgüler, M.E., Turgay, M.I., Sahin, H., 1984. Geophysical Investigation in Denizli Geothermal Fields. Bulletin of the Mineral Research and Exploration Institute of Turkey 99-100, 129–141.
Özkul, M., Varol, B., Alçiçek, M.C., 2002. Depositional environments and petrography of the Denízlí travertines. Bulletin of the Mineral Research and Exploration 125, 13–29.
Özkul, M., Gökgöz, A., Horvatinčić, N., 2010. Depositional properties and geochemistry of Holocene perched springline tufa deposits and associated spring waters: a case study from the Denizli Province, Western Turkey. Geological Society, London, Special Publications 336, 245–262.
Price, S.P., Scott, B., 1994. Fault-block rotations at the edge of a zone of continental extension; southwest Turkey. Journal of Structural Geology 16, 381–392.
Röller, K., Trepmann, C.A., 2003. Stereo32 version 1.0.2. Ruhr Universität Bohum.
Secor, D.T., 1965. Role of fluid pressure in jointing. American Journal of Sciences 263, 633–646.
Sintubin, M., Muchez, Ph., Similox-Tohon, D., Verhaert, G., Paulissen, E., Waelkens, M., 2003. Seismic catastrophes at the ancient city of Sagalassos (SW Turkey) and their implications for seismotectonics in the Burdur–Isparta area. Geological Journal 38, 359–374.
Stewart, I.S., Hancock, P.L., 1990. Brecciation and fracturing within neotectonic normal fault zones in the Aegean region. In: Knipe, R.J., Rutter, E.H. (Eds.), Deformation Mechanisms, Rheology and Tectonics, Geological Society, London, Special Publications, 54, pp. 105–110.
Taymaz, T., Price, S., 1992. The 1971 May 12 Burdur Earthquake sequence, SW Turkey — a synthesis of seismological and geological observations. Geophysical Journal International 108, 589–603.
Uysal, I.T., Feng, Y., Zhao, J.-X., Isik, V., Nuriel, P., Golding, S.D., 2009. Hydrothermal $CO_2$ degassing in seismically active zones during the late Quaternary. Chemical Geology 265, 442–454.
van Hinsbergen, D.J.J., Kaymakci, N., Spakman, W., Torsvik, T.H., 2010. Reconciling the geological history of western Turkey with plate circuits and mantle tomography. Earth and Planetary Science Letters 297, 674–686.
Van Noten, K., Sintubin, M., 2010. Linear to non-linear relationship between vein spacing and layer thickness in centimetre- to decimetre-scale siliciclastic multilayers from the High-Ardenne slate belt (Belgium, Germany). Journal of Structural Geology 32, 377–391.
Van Noten, K., Muchez, Ph., Sintubin, M., 2011. Stress-state evolution of the brittle upper crust during compressional tectonic inversion as defined by successive quartz vein types (High-Ardenne slate belt, Germany). Journal of the Geological Society of London 168, 407–422.
Van Noten, K., Van Baelen, H., Sintubin, M., 2012. The complexity of 3D stress-state changes during compressional tectonic inversion at the onset of orogeny. In: Healy, D., Butler, R.W.H., Shipton, Z.K., Sibson, R.H. (Eds.), Faulting, Fracturing, and Igneous Intrusion in the Earth's crust: Geological Society, London, Special Publications, 367, pp. 51–69.
Verhaert, G., Muchez, Ph., Sintubin, M., Similox-Tohon, D., Vandycke, S., Keppens, E., Hodge, E.J., Richards, D.A., 2004. Origin of palaeofluids in a normal fault setting in the Aegean region. Geofluids 4, 300–314.
Verhaert, G., Similox-Tohon, D., Vandycke, S., Sintubin, M., Muchez, Ph., 2006. Different stress states in the Burdur-Isparta region (SW Turkey) since Late Miocene times: a reflection of a transient stress regime. Journal of Structural Geology 28, 1067–1083.
Wallace, R.E., 1951. Geometry of shearing stress and relation to faulting. Journal of Geology 69, 118–130.
Westaway, R., 1993. Neogene evolution of the Denizli region of western Turkey. Journal of Structural Geology 15, 37–53.
Westaway, R., Guillou, H., Yurtmen, S., Demir, T., Scaillet, S., Rowbotham, G., 2005. Constraints on the timing and regional conditions at the start of the present phase of crustal extension in western Turkey, from observations in and around the Denizli region. Geodinamica Acta 18, 209–238.
Yagiz, S., 2010. Geomechanical properties of construction stones quarried in Southwestern Turkey. Scientific Research and Essays 5, 750–757.